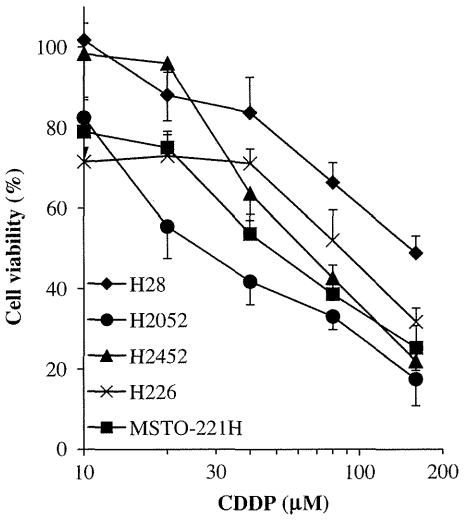

Fig. 1. Susceptibility of malignant mesothelioma cells to CDDP. Mesothelioma cells, H28, H2052, H2452, H226 and MSTO-221H were cultured with various concentrations of CDDP for 24 h 37 °C under 5% CO_2. Cell viability was assayed using the WST-8 assay. Maximal cell viability (100%) was obtained by incubating cells without CDDP. Data are shown as means and standard deviations ($n = 4$).

3.2. Identification of differentially expressed proteins by 2D-DIGE and MS

In order to search for CDDP susceptibility-related proteins, differential proteome analysis between H2052 and H28 cell lines was performed to search for CDDP susceptibility-related proteins (Fig. 2). Quantitative image analysis indicated that a total of eight protein spots representing > 2.0-fold alteration in expression were found and then identified by MS analysis (Table 1). Among those eight proteins, we focused on ANXA4 because this protein plays an important role in membrane stability. Previous reports have indicated that ANXA4 is associated with chemoresistance against platinum-based anticancer drugs in human lung, colon [13] and ovarian cancer [14].

3.3. ANXA4 expression analysis in human malignant mesothelioma cells and mesothelial tissues

Correlations between the expression levels in five malignant mesothelioma cell lines with CDDP-susceptibility were examined using western blot analysis to validate the identified proteins as CDDP susceptibility-related proteins. ANXA4 was expressed at a higher level in H28 cells relative to the other four CDDP-susceptible malignant mesothelioma cell lines (Fig. 3A and B). Expression of ANXA4 in human mesothelial tissue was analyzed by immunohistochemistry staining with an anti-human ANXA4 monoclonal antibody. Fig. 3C indicates that ANXA4 was expressed at higher levels in human malignant mesothelioma tissues than in benign mesothelioma tissues and normal mesothelial tissues.

3.4. Gene regulation of ANXA4 in malignant mesothelioma cells by knockdown and overexpression

ANXA4-siRNA and ANXA4-pcDNA 3.1 were next transfected to H28 and H2052 before CDDP treatment to evaluate correlations between ANXA4 expression levels and CDDP susceptibility. The IC_{50} values of [H28/non treat: H28/control-siRNA: H28/ANXA4-siRNA] were [80.0 μM: 71.8 μM: 15.5 μM] and [H2052/control-pcDNA 3.1: [H2052/ANXA4-pcDNA 3.1] were [55.2 μM: 89.7 μM], respectively (Fig. 4A–D). These results suggested that the CDDP susceptibility of H28 cells was increased by ANXA4-siRNA transfection and that of H2052 cells was decreased by ANXA4-pcDNA 3.1 transfection.

4. Discussion

In this study, a proteomic analysis was performed based on 2D-DIGE using malignant mesothelioma cell lines to identify candidate proteins associated with CDDP susceptibility (Figs. 1 and 2). Eight proteins that were differentially expressed in H28 cells compared with H2052 cells were identified (Table 1). ANXA4 was found to be expressed at a higher level in H28 cells relative to levels in CDDP-susceptible malignant mesothelioma cells by western blot

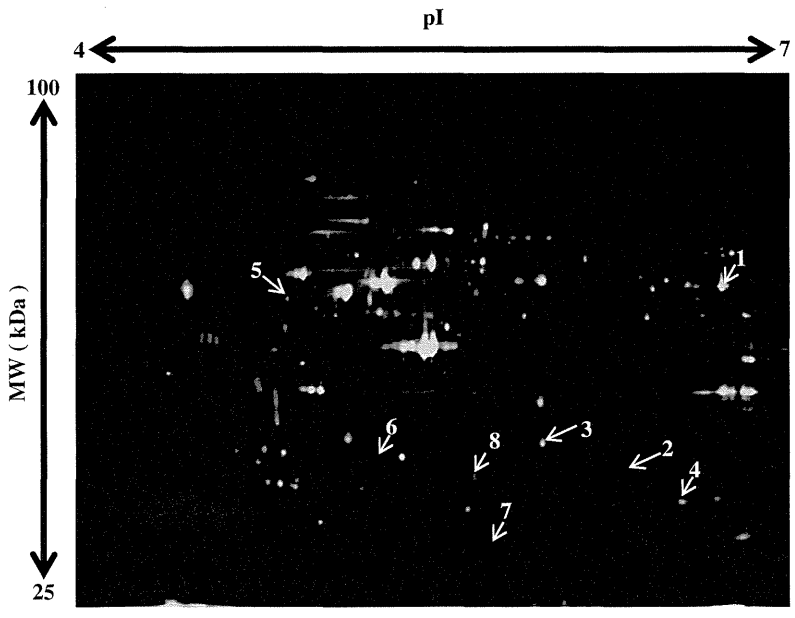

Fig. 2. 2D-DIGE image of fluorescently labeled proteins from human mesothelioma cell lines H28 and H2052. Proteins from high- and low-susceptible mesothelioma cells (H2052, H28) were labeled with cy3 and cy5, respectively, and 2D electrophoresis was performed. The differentially expressed spots in H28 indicated by white arrows were then identified by LC-TOF-MS/MS. Table 1 contains additional information about the identified proteins.

Table 1
Proteins expressed at higher or lower levels in H28 compared to H2052.

No.	Accession number	Protein name	pI	MW (kDa)	Expression ratio (H28/H2052)
1	P11413	Glucose-6-phosphate 1-dehydrogenase	6.4	59.3	21.0
2	P78417	Glutathione *S*-transferase omega-1	6.2	27.6	7.4
3	P09525	Annexin A4	5.6	35.9	3.6
4	P30041	Peroxiredoxin-6	6.0	25.0	3.5
5	Q09028	Histone-binding protein RBBP4	4.7	47.7	3.0
6	P07195	L-lactate dehydrogenase B chain	5.7	36.6	2.9
7	P32119	Peroxiredoxin-2	5.7	21.9	0.03
8	Q9Y696	Chloride intracellular channel protein 4	5.5	28.8	0.13

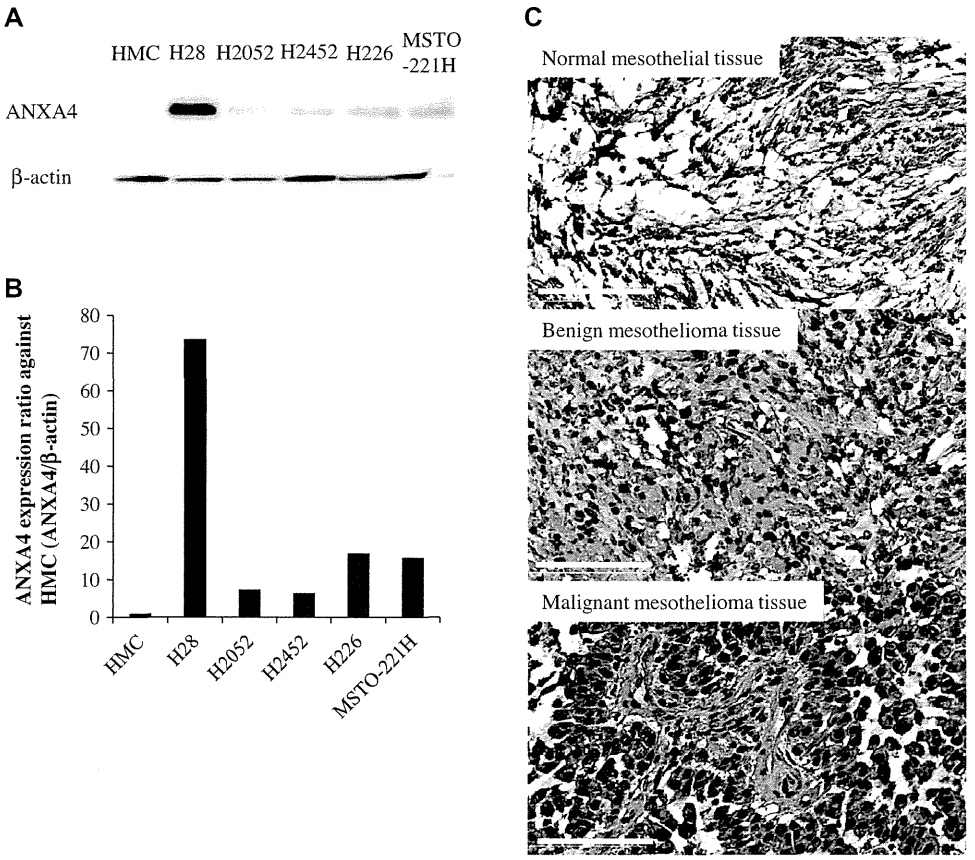

Fig. 3. ANXA4 expression analysis in human malignant mesothelioma cells and mesothelial tissues. ANXA4 expression levels in human primary mesothelial cells, HMC, and mesothelioma cell lines (H28, H2052, H2452, H226, MSTO-221H) were analyzed by western blotting (A). Intensity of the western blotting images was quantified by densitometry (B). Expression of ANXA4 in human mesothelial tissues was analyzed by immunostaining using an anti-human ANXA4 antibody (C). Top, middle and bottom panels are normal mesothelial, benign and malignant mesothelioma tissues, respectively. The tissue sections were counterstained using hematoxylin. Representative 400 × photomicrographs presented (bar: 100 μm).

analysis (Fig. 3A and B). Furthermore, ANXA4 was expressed in malignant mesothelioma tissue but not in benign mesothelial tumor and normal mesothelial tissues (Fig. 3C). Thus, ANXA4 was expressed in CDDP-susceptible malignant mesothelioma cells and specifically in malignant mesothelioma tissues. These results indicate that ANXA4 expression in malignant mesothelioma cells may be correlated with CDDP susceptibility, although this relationship must be validated in future studies of human clinical malignant mesothelial cases. The CDDP susceptibility of H28 cells was actually increased by ANXA4 knockdown, and that of H2052 cells was decreased by ANXA4 overexpression (Fig. 4). Thus, these results suggest that ANXA4 plays an important role in chemoresistance against CDDP.

ANXA4 has already been characterized as a regulator of cell membranes with calcium dependency [15–17]. Recently, some studies have reported the protein is associated with membrane permeability [18], ion channels [19] and exocytosis [20,21]. These observations may explain in part the correlation of ANXA4 with modulation of drug susceptibility in cancer cells.

This study demonstrates for the first time elevated ANXA4 protein expression in malignant mesothelioma cells that have less susceptibility to CDDP. *In vitro* evaluation of drug susceptibility against CDDP in malignant mesothelioma cells derived from cancer patients would be important in clinical conditions because doctors as well as patients wish to avoid treatment with inefficacious drugs. Consequently, the susceptibility of a given patient against CDDP could be confirmed by analyzing the expression level of ANXA4 in malignant mesothelioma patients at the time of diagnosis. Furthermore, if ANXA4 expression could be blocked specifically in malignant mesothelioma cells by nucleic acid drugs such as siRNA, this procedure would prove useful in clinical situations involving CDDP treatment. The present study may contribute to

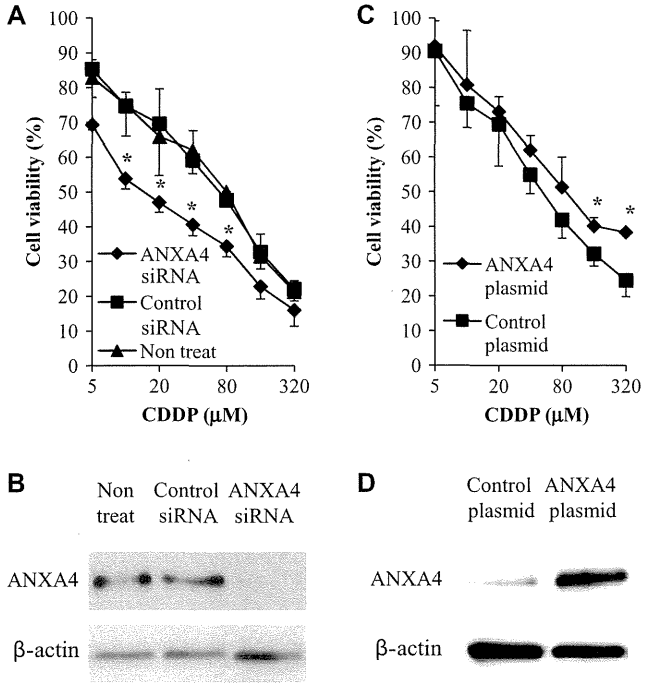

Fig. 4. The effect of ANXA4 gene knockdown and overexpression on CDDP susceptibility in malignant mesothelioma cells. Transfection of ANXA4 siRNA or plasmid into malignant mesothelioma cells confers resistance to CDDP. Cell survival after 24 h treatment of H28/ANXA4 siRNA or H2052/ANXA4 plasmid with different concentrations of CDDP (A and C). Expression of ANXA4 was analyzed by western blot analysis (B and D). Data are shown as means and standard deviations ($n = 4$). *$P < 0.05$ (Control siRNA or plasmid vs. ANXA4 siRNA or plasmid).

establishment of a new therapeutic strategy for malignant mesothelioma patients by suggesting a novel diagnostic and therapeutic target.

Acknowledgments

This study was supported in part by Grants-in-Aid for Scientific Research from the Ministry of Education, Culture, Sports, Science and Technology of Japan, and from the Japan Society for the Promotion of Science (JSPS). This study was also supported in part by Health Labor Sciences Research Grants from the Ministry of Health, Labor and Welfare of Japan and by Health Sciences Research Grants for Research on Publicly Essential Drugs and Medical Devices from the Japan Health Sciences Foundation.

References

[1] W.N. Rom, W.D. Travis, A.R. Brody, Cellular and molecular basis of the asbestos-related diseases, Am. Rev. Respir. Dis. 143 (1991) 408–422.
[2] N.H. Heintz, Y.M. Janssen-Heininger, B.T. Mossman, Asbestos, lung cancers, and mesotheliomas: from molecular approaches to targeting tumor survival pathways, Am. J. Respir. Cell Mol. Biol. 42 (2010) 133–139.
[3] Consensus Report: Asbestos, asbestosis, and cancer: the Helsinki criteria for diagnosis and attribution. Scand. J. Work Environ. Health 23 (1997) 311–316.
[4] T.D. Yan, L. Welch, D. Black, P.H. Sugarbaker, A systematic review on the efficacy of cytoreductive surgery combined with perioperative intraperitoneal chemotherapy for diffuse malignancy peritoneal mesothelioma, Ann. Oncol. 18 (2007) 827–834.
[5] E. Chailleux, D. Pioche, S. Chopra, G. Dabouis, P. Germaud, A.Y. De Lajartre, M. De Lajartre, Prognostic factors in diffuse malignant pleural mesothelioma: a study of 167 patients, Chest 93 (1988) 159–162.
[6] K.S. Sridhar, R. Doria, W.A. Raub Jr., R.J. Thurer, M. Saldana, New strategies are needed in diffuse malignant mesothelioma, Cancer 70 (1992) 2969–2979.
[7] M. Markman, D. Kelsen, Efficacy of cisplatin-based intraperitoneal chemotherapy as treatment of malignant peritoneal mesothelioma, J. Cancer Res. Clin. Oncol. 118 (1992) 547–550.
[8] G.H. Eltabbakh, M.S. Piver, R.E. Hempling, F.O. Recio, M.E. Intengen, Clinical picture, response to therapy, and survival of women with diffuse malignant peritoneal mesothelioma, J. Surg. Oncol. 70 (1999) 6–12.
[9] T. Berghmans, M. Paesmans, Y. Lalami, I. Louviaux, S. Luce, C. Mascaux, A.P. Meert, J.P. Sculier, Activity of chemotherapy and immunotherapy on malignant mesothelioma: a systematic review of the literature with meta-analysis, Lung. Cancer 38 (2002) 111–121.
[10] H.J. Lerner, D.A. Schoenfeld, A. Martin, G. Falkson, E. Borden, Malignant mesothelioma: The Eastern Cooperative Oncology Group (ECOG) experience, Cancer 52 (1983) 1981–1985.
[11] D.M. Mintzer, D. Kelsen, D. Frimmer, R. Heelan, R. Gralla, Phase II trial of high-dose cisplatin in patients with malignant mesothelioma, Cancer Treat Rep. 69 (1985) 711–712.
[12] B.L. Zidar, S. Green, H.I. Pierce, R.W. Roach, S.P. Balcerzak, L. Militello, A phase II evaluation of cisplatin in unresectable diffuse malignant mesothelioma: a Southwest Oncology Group Study, Invest New Drugs 6 (1988) 223–226.
[13] E.K. Han, S.K. Tahir, S.P. Cherian, N. Collins, S.C. Ng, Modulation of paclitaxel resistance by annexin IV in human cancer cell lines, Br. J. Cancer 83 (2000) 83–88.
[14] A. Kim, T. Enomoto, S. Serada, Y. Ueda, T. Takahashi, B. Ripley, T. Miyatake, M. Fujita, C.M. Lee, K. Morimoto, M. Fujimoto, T. Kimura, T. Naka, Enhanced expression of Annexin A4 in clear cell carcinoma of the ovary and its association with chemoresistance to carboplatin, Int. J. Cancer 125 (2009) 2316–2322.
[15] M.A. Kaetzel, P. Hazarika, J.R. Dedman, Differential tissue expression of three 35-kDa annexin calcium-dependent phospholipid-binding proteins, J. Biol. Chem. 264 (1989) 14463–14470.
[16] G. Zanotti, G. Malpeli, F. Gliubich, C. Folli, M. Stoppini, L. Olivi, A. Savoia, R. Berni, Structure of the trigonal crystal form of bovine annexin IV, Biochem. J. 329 (1998) 101–106.
[17] M.A. Kaetzel, Y.D. Mo, T.R. Mealy, B. Campos, W. Bergsma-Schutter, A. Brisson, J.R. Dedman, B.A. Seaton, Phosphorylation mutants elucidate the mechanism of annexin IV-mediated membrane aggregation, Biochemistry 40 (2001) 4192–4199.
[18] W.G. Hill, M.A. Kaetzel, B.K. Kishore, J.R. Dedman, M.L. Zeidel, Annexin A4 reduces water and proton permeability of model membranes but does not alter aquaporin 2-mediated water transport in isolated endosomes, J. Gen. Physiol. 121 (2003) 413–425.
[19] M.A. Kaetzel, H.C. Chan, W.P. Dubinsky, J.R. Dedman, D.J. Nelson, A role for annexin IV in epithelial cell function. Inhibition of calcium-activated chloride conductance, J. Biol. Chem. 269 (1994) 5297–5302.
[20] H. Sohma, C.E. Creutz, S. Gasa, H. Ohkawa, T. Akino, Y. Kuroki, Differential lipid specificities of the repeated domains of annexin IV, Biochim. Biophys. Acta 1546 (2001) 205–215.
[21] A. Piljic, C. Schultz, Annexin A4 self-association modulates general membrane protein mobility in living cells, Mol. Biol. Cell 17 (2006) 3318–3328.

Neuroscience Letters 534 (2013) 85–89

Contents lists available at SciVerse ScienceDirect

Neuroscience Letters

journal homepage: www.elsevier.com/locate/neulet

Proteomic analysis of the hippocampus in Alzheimer's disease model mice by using two-dimensional fluorescence difference in gel electrophoresis

Masaoki Takano[a], Takuya Yamashita[b,c], Kazuya Nagano[c], Mieko Otani[a], Kouji Maekura[a], Haruhiko Kamada[c], Shin-ichi Tsunoda[c], Yasuo Tsutsumi[b,c], Takami Tomiyama[e,f], Hiroshi Mori[e,f], Kenji Matsuura[d], Shogo Matsuyama[d,*]

[a] Laboratory of Molecular Cellular Biology, School of Pharmaceutical Sciences, Kobe Gakuin University, 1-1-3 Minatojima, Chuo-ku, Kobe 650-8586, Japan
[b] Laboratory of Toxicology and Safety Science, Graduate School of Pharmaceutical Sciences, Osaka University, 1-6 Yamadaoka, Suita, Osaka 565-0871, Japan
[c] Laboratory of Biopharmaceutical Research, National Institute of Biomedical Innovation, 7-6-8 Saito-Asagi, Ibaraki, Osaka 567-0085, Japan
[d] Faculty of Pharmaceutical Sciences, Himeji Dokkyo University, 7-2-1 Kamiohno, Himeji 670-8524, Japan
[e] Department of Neuroscience, Osaka City University Graduate School of Medicine, Osaka 545-8585, Japan
[f] Core Research for Evolutional Science and Technology, Japan Science and Technology Agency, Japan

HIGHLIGHTS

- We perform the proteome for $APP_{E693\Delta}$-transgenic mice. Methods are two-dimensional fluorescence difference in gel electrophoresis and mass spectrometry techniques. The expression of 14 proteins are changed in the brain. Aβ oligomers contribute to the expression of proteins.

ARTICLE INFO

Article history:
Received 4 August 2012
Received in revised form 13 October 2012
Accepted 6 November 2012

Keywords:
Proteome
Amyloid β oligomers
Alzheimer's disease
Hippocampus
2D-DIGE

ABSTRACT

We previously identified the E693Δ mutation in amyloid precursor protein (APP) in patients with Alzheimer's disease (AD) and then generated APP-transgenic mice expressing this mutation. As these mice possessed abundant Aβ oligomers from 8 months of age but no amyloid plaques even at 24 months of age, they are a good model to study pathological effects of amyloid β (Aβ) oligomers. The two-dimensional fluorescence difference in gel electrophoresis (2D-DIGE) technology, using a mixed-sample internal standard, is now recognized as an accurate method to determine and quantify proteins. In this study, we examined the proteins for which levels were altered in the hippocampus of 12-month-old $APP_{E693\Delta}$-transgenic mice using 2D-DIGE and liquid chromatography–tandem mass spectrometry (LC–MS/MS). Fourteen proteins were significantly changed in the hippocampus of $APP_{E693\Delta}$-transgenic mice. Actin cytoplasmic 1 (β-actin), heat shock cognate 71 kDa, γ-enolase, ATP synthase subunit β, tubulin β-2A chain, clathrin light chain B (clathrin) and dynamin-1 were increased. Heat shock-related 70 kDa protein 2, neurofilament light polypeptide (NFL), stress-induced-phosphoprotein 2, 60 kDa heat shock protein (HSP60), α-internexin, protein kinase C and casein kinase substrate in neurons protein 1 (Pacsin 1), α-enolase and β-actin were decreased. Western blotting also validated the changed levels of HSP60, NFL, clathrin and Pacsin 1 in $APP_{E693\Delta}$-transgenic mice. The identified proteins could be classified as cytoskeleton, chaperons, neurotransmission, energy supply and signal transduction. Thus, proteomics by 2D-DIGE and LC–MS/MS has provided knowledge of the levels of proteins in the early stages of AD brain.

1. Introduction

AD is neuropathologically characterized by abnormal accumulation of extracellular amyloid plaques and intracellular neurofibrillary tangles throughout cortical and limbic regions. Although the current amyloid cascade hypothesis [6] and tau hypothesis [15] provide frameworks for studying AD pathogenesis. Recently, diverse lines of evidence suggest that Aβ peptides play more important roles in AD pathogenesis [13,16,20]. Especially, soluble oligomers of Aβ could be a cause of synaptic and cognitive dysfunction in the early stages of AD. To address the relationship between Aβ oligomers and pathological features of AD, we generated APP transgenic mice expressing the E693Δ mutation, which enhanced Aβ oligomerization without fibrillization [25]. It might provide a clue for elucidating AD pathology caused by Aβ oligomers to analyze the $APP_{E693\Delta}$-transgenic mice.

* Corresponding author. Tel.: +81 79 223 6849; fax: +81 79 223 6857.
E-mail address: shogo@himeji-du.ac.jp (S. Matsuyama).

0304-3940/$ – see front matter © 2012 Elsevier Ireland Ltd. All rights reserved.
http://dx.doi.org/10.1016/j.neulet.2012.11.010

One of the most utilized approaches in proteomics to quantify and identify proteins is two dimensional gel electrophoresis (2DE) and mass spectrometry (MS) [5]. Proteomic approaches were most widely based on methods using differential expression on 2D-PAGE gels, or more recently 2D chromatography, followed by mass spectrometry protein identification. Compared to these conventional analyses, 2D-DIGE has higher reproducibility and sensitivity because of its internal standard design which minimizes gel-to-gel variation, improves spot matching, reduces number of gels needed, and permits quantitative analysis of small sample amounts.

In this study, we studied the altered expression of proteins in the hippocampus of $APP_{E693\Delta}$-transgenic mice using 2D-DIGE and LC–MS/MS approach. This approach revealed that the levels of at least 14 proteins were altered in the hippocampus of 12-month-old $APP_{E693\Delta}$-transgenic mice. These findings suggest that Aβ oligomers might cause synaptic and cognitive dysfunction by affecting the expression of these proteins in the hippocampus.

2. Experimental procedures

2.1. Materials

Sodium dodecyl sulfate, urea, thiourea, CHAPS, dithiothreitol, iodoacetamide, bromophenol blue, and RNase A and DNase I for SDS-PAGE or 2DE were all obtained from Wako Pure Chemical Industries (Osaka, Japan). Source information for all other assay reagents and materials are incorporated into their respective assay methods described below.

2.2. Animal subjects

Transgenic mice expressing human APP_{695} with the APP E693Δ mutation under the mouse prion promoter were used [25]. Heterozygous human $APP_{E693\Delta}$-transgenic mice and age-matched non-transgenic littermates were sacrificed at 12 months of age, and their hippocampi were isolated on an ice-cold plate. Animal care and handling were performed strictly in accordance with the Guidelines for Animal Experimentation at Kobe Gakuin University and Himeji Dokkyo University. Every effort was made to minimize the number of animals used and their suffering.

2.3. Protein labeling with CyDyes

Equal amounts of total protein from 4 hippocampi of $APP_{E693\Delta}$-transgenic mice or age-matched non-transgenic littermates were separately pooled. Protein samples were labeled with CyDyes (GE Healthcare, Piscataway, NJ), as per manufacturer's instructions. In brief, 50 μg of total protein from each sample was mixed in a tube and labeled with Cy2 minimal dye, and 50 μg protein taken from the mix was used as an internal standard on each gel for the three subsequent 2DE and image analysis. In parallel, 50 μg protein from each sample was labeled with either Cy3 or Cy5, and the dyes scrambled within each group to avoid possible dye bias. As a result, one replicate was Cy3 labeled proteins and another replicate was Cy5 labeled proteins. Two replicates (Cy3 and Cy5 labeled samples) were mixed, divided and applied each three independent gels. The sample volumes were adjusted to 18 μL with labeling buffer (7M urea, 2 M thiourea, 4% CHAPS, 30 mM Tris), followed by addition of 1 μL dye (working solution) to each individual sample. The samples were left on ice for 30 min in the dark, followed by adding 1 μL of 10 mmol/L lysine to stop the reaction.

2.4. 2D electrophoresis and image analysis

One sample from each of the CyDye groups was mixed together and adjusted to final concentrations of 1% DTT, 1% IPG buffer at a total volume of 350 μL with lysis buffer (7 M urea, 2 M thiourea, 4% CHAPS) and was used to 24 cm pH 4–7 IPG strips (non-linear; GE Healthcare, Piscataway, NJ) overnight. First dimension isoelectric focusing (IEF) was carried out with IPGphor II (GE Healthcare, Piscataway, NJ). Second dimension SDS-PAGE was performed by mounting the IPG strips onto 20 × 26 cm 12.5% DIGE gels (GE Healthcare, Piscataway, NJ) using Ettan DALT six Large Electrophoresis System (GE Healthcare, Piscataway, NJ) and running the gels at 16 mA/gel for the initial hour and 25 mA/gel at 25 °C constantly until bromophenol blue reached the bottom of the gel. The lysates were labeled at the ratio of 50 μg proteins: 400 pmol Cy3 or Cy5 protein-labeling dye (GE HealthcareBiosciences) in dimethylformamide according to the manufacturer's protocol.

In summary, three analytical gels were completed in total, running 25 μg of pooled reference sample labeled with Cy2, along with two samples (25 μg each), one labeled with Cy3 and the other labeled with Cy5. Gels selected for picking were stained with Deep purple (GE Healthcare, Piscataway, NJ). Approximately 1100 spots were matched across all three analytical gels. The analytical gel was picked using an automated robotic system, Ettan Spot picker (GE Healthcare, Piscataway, NJ). The pick list was created based on the Deep purple image. 2 mm gel plugs were picked, washed, reduced and alkylated, and then digested with trypsin, and the resulting peptides were extracted. Gel trypsinization was performed as previously described [24].

2.5. LC/MS/MS identification

Trypsinized peptides were analyzed by nano LC/MS/MS on a ThermoFisher LTQ Orbitrap XL. In brief, 30 mL of hydrolysate was loaded onto a 5 mm 675 mm ID C12 (Jupiter Proteo, Phenomenex) vented column at a flow-rate of 10 mL/min. Gradient elution was conducted on a 15 cm by 75 mm ID C12 column at 300 nL/min. A 30 min gradient was employed. The mass spectrometer was operated in a data-dependent mode, and the six most abundant ions were selected for MS/MS. Mass spectrometry results were searched using Mascot (www.matrixscience.com). Samples were processed in the Scaffold algorithm using DAT files generated by Mascot. Parameters for LTQ Orbitrap XL data require a minimum of two peptide matches per protein with minimum probabilities of 90% at the protein level.

2.6. Western blotting

Approximately 25 μg of protein from mouse hippocampus was applied to a 12.5% acrylamide gel and SDS-polyacrylamide gel electrophoresis was performed at 17.5 mA/gel for 2 h in second dimension. The gels were transferred onto PVDF membranes (Pall Corporation, Pensacola, FL, USA), in a trans-blot electrophoresis transfer cell (Nihon Eido, Tokyo, Japan). Western blotting was performed by using monoclonal antibodies against β-actin (diluted 1:1000, Cell Signaling, USA) and clathrin (diluted 1:250, Abcam, USA), polyclonal antibodies HSP60, NFL, voltage-dependent anion-selective channel protein 1 (VDAC) (diluted 1:1000, Cell Signaling, USA) and Pacsin 1 (diluted 1:500, Millipore, USA). Peroxidase-conjugated antibody (diluted 1:5000, Abcam, USA) was used as secondary antibody. The reaction was detected by chemiluminescence with ECL reagents (Pierce Biotechnology, USA). A semi quantitative analysis based on optical density was performed by ImageJ software (available at http://www.rsbweb.nih.gov/ij).

3. Results and discussion

The 2D-DIGE gels of the hippocampi from wild type and $APP_{E693\Delta}$-transgenic mice pools were shown as Fig. 1. Two replicates of each pooled sample were run, labeling one replicate with

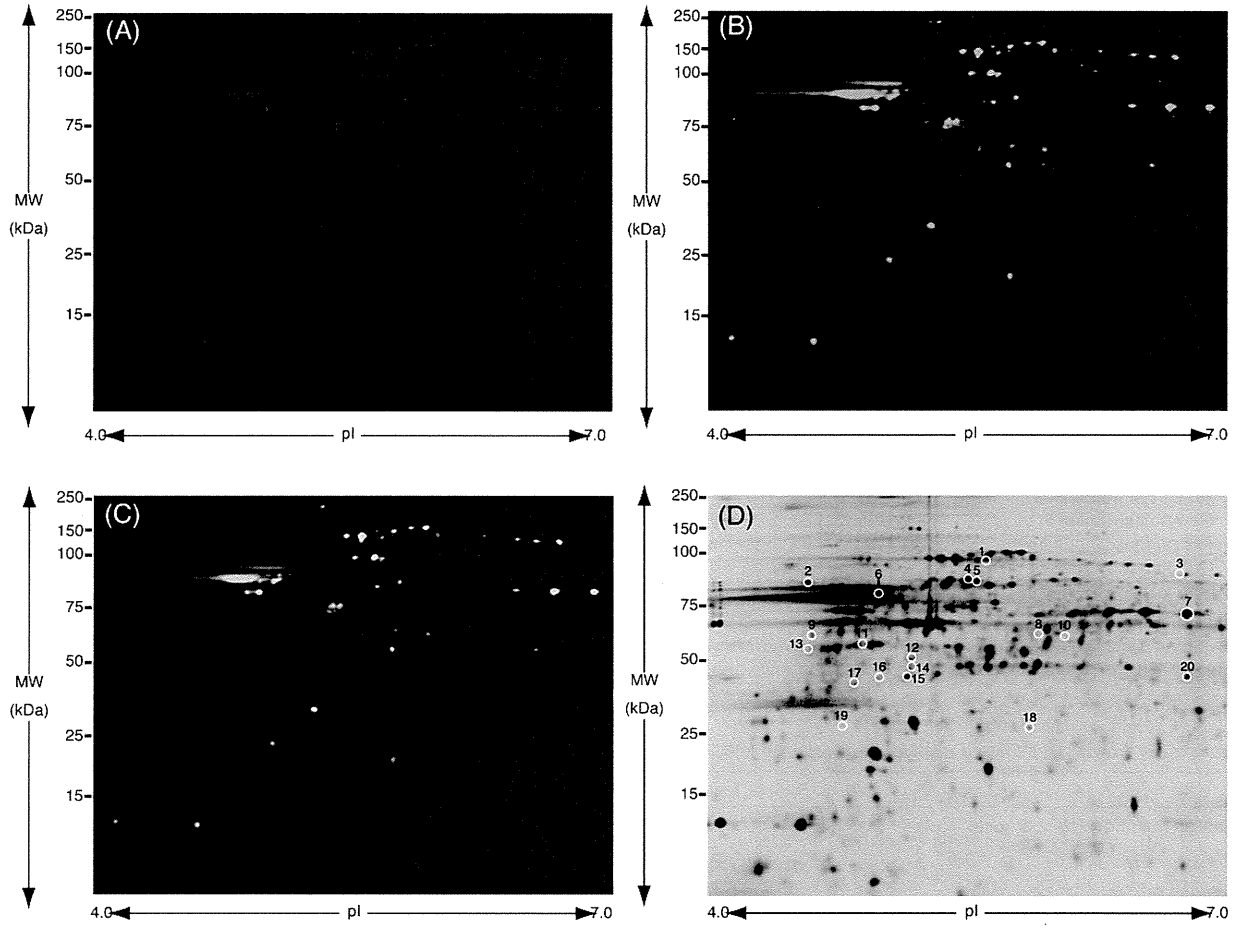

Fig. 1. 2D-DIGE gel image of fluorescence-labeled hippocampal proteins of non-transgenic and $APP_{E693\Delta}$-transgenic mice. (A) Analysis of the proteome of non-transgenic mice hippocampi with Cy3 Dye. (B) $APP_{E693\Delta}$-transgenic mice hippocampi with Cy5 Dye. (C) Merged. (D) Fourteen protein spots identified from non-transgenic and $APP_{E693\Delta}$-transgenic mice hippocampi by LC/MS/MS. Black numbers with white circles indicate proteins that are listed in Table 1.

Cy3 (Fig. 1A) and one replicate with Cy5 (Fig. 1B), resulting in three analytical gels. The 2D-DIGE comparative analysis of the wild type and $APP_{E693\Delta}$-transgenic mice revealed significant 74 spots (Fig. 1C). These spots were investigated by LC–MS/MS (Fig. 1D). Finally, fourteen proteins were identified as shown in Table 1. These proteins are classified into several groups that are involved in cytoskeletal, chaperone, energy metabolic, vesicle transport and signaling proteins (Table 2).

Spot nos. 1, 3 and 4 were identified as heat shock-related 70 kDa protein 2, stress-induced-phosphoprotein 1 and HSP60, respectively. The stress-induced-phosphoprotein 1 is the co-chaperone and thought of the function in regulation of interaction with Hsp70 and Hsp90 [10]. HSP60 is the chaperonin which is implicated in mitochondrial protein import and macromolecular assembly and may facilitate the correct folding of imported proteins [9]. The amounts of heat shock-related 70 kDa protein 2, stress-induced-phosphoprotein 1, and HSP60 were significantly decreased. On the contrary, spot no. 9 which was identified as heat shock cognate 71 kDa protein was significantly increased. This protein is also the chaperone and acts as a repressor of transcriptional activation [8]. Thus, Aβ oligomers might contribute to changing the expression of the chaperons.

Spot nos. 8, 10–12 and 16 were identified as actin, and spot nos. 15 and 17 were identified as tubulin β-2A chain. Actin is one of the major cytoskeletal proteins in neurons, and the dynamics of its assembly are involved in many aspects of cell motility, vesicle transport, and membrane turnover [14]. Actin itself is known to link with Aβ, which enhances the neurotoxicity induced by tau-mediated actin filament formation [4]. The four spots of actin but not no. 12 and those of tubulin were significantly increased. Thus, Aβ oligomers might lead to increasing the amounts of actin and tubulin.

Spot nos. 5 and 2 were identified as α-internexin and NFL, respectively, which are known as neuronal intermediate proteins [2,18]. The amounts of α-internexin and NFL were significantly decreased. Thus, the decreased amounts of NFL and internexin might raise neural dysfunction in the hippocampus of AD.

Spot nos. 7 and 13 were identified as α-enolase. Spot nos. 14 and 19 were identified as γ-enolase and ATP synthase subunit β, respectively. Enolase is a multifunctional protein as glycolytic enzyme, belonging to a novel class of surface proteins [11]. ATP synthase is a key role enzyme that provides energy for the cell to use through the synthesis of ATP [1]. The amount of α-enolase was significantly decreased, but the amounts of γ-enolase and ATP synthase subunit β were significantly increased. Interestingly, the levels of α-enolase and ATP synthase subunit α mitochondrial proteins significantly increased in the hippocampus of J20 Tg mice with amyloid deposition [19]. The amyloid deposit enhanced the expression of energy metabolic proteins [22]. Combined with our findings, both Aβ oligomers and amyloid deposition might play an important role in the change of energy metabolic proteins as α-enolase, γ-enolase and ATP synthase subunit β.

Spot no. 20 was identified as dynamin. Dynamin, a well studied neuron-specific mechanochemical GTPase, pinches off synaptic vesicles, freeing them from the membrane and allowing them to re-enter the synaptic vesicle pool to be refilled for future release

Table 1
Identified proteins from differentially expressed in the hippocampus of$APP_{E693\Delta}$-transgenic mice when compared to non-transgenic littermates.

Spot no.	Protein ID	Fold (APP/WT)	*t*-Test	Accession	Coverage	#Peptides	Predicted MW (kDa)	Calc. pI	Score
1	Heat shock-related 70 kDa protein 2	−1.32	0.040	P14659	26.22	23	69.6	5.67	625.70
2	Neurofilament light polypeptide	−1.48	0.002	P08551	39.96	43	61.5	4.64	1004.84
3	Stress-induced-phosphoprotein 1	−1.44	0.002	Q60864	16.21	9	62.5	6.80	157.49
4	60 kDa heat shock protein	−1.36	0.013	P63038	52.71	71	60.9	6.18	1916.39
5	Alpha-internexin	−1.34	0.023	P46660	42.66	39	55.7	5.27	1119.47
6	Protein kinase C and cascin kinase substrate in neurons protein 1	−1.48	0.023	Q61644	28.34	15	50.5	5.24	356.92
7	Alpha-enolase	−1.32	0.000	P17182	34.33	24	47.1	6.80	474.21
8	Actin, cytoplasmic 1	1.51	0.003	P60709	25.87	14	41.7	5.48	231.79
9	Heat shock cognate 71 kDa protein	1.35	0.015	P63017	12.54	16	70.8	5.52	319.85
10	Actin, cytoplasmic	1.34	0.004	P60709	24.27	13	41.7	5.48	279.37
11	Actin, cytoplasmic 1	1.38	0.022	P60709	15.47	7	41.7	5.48	243.14
12	Actin, cytoplasmic 1	−1.56	0.013	P60709	22.67	12	41.7	5.48	131.57
13	Gamma-enolase	1.33	0.005	P17183	20.05	13	47.3	5.11	237.25
14	ATP synthase subunit beta	1.40	0.047	P56480	23.60	18	56.3	5.34	356.19
15	Tubulin beta-2A chain	1.31	0.021	Q13885	14.83	13	49.9	4.89	313.07
16	Actin, cytoplasmic 1	1.47	0.002	P60709	6.93	3	41.7	5.48	97.01
17	Tubulin beta-2S chain	1.44	0.009	Q13885	11.46	5	49.9	4.89	118.50
18	Clathrin light chain B	1.68	0.005	P09497	8.30	3	25.2	4.64	95.06
19	ATP synthase subunit beta	1.46	0.013	P06576	16.64	16	56.5	5.40	283.06
20	Dynamin-1	1.40	0.006	Q05193	9.61	13	97.3	7.17	242.16

Mass spectrometry protein identification of 2D-DIGE spots of interest and statistical analysis using *t*-test between wild type mice and $APP_{E693\Delta}$-transgenic mice gels ($P < 0.05$). The proteins of mouse hippocampus were separated by 2DE and identified by LC MS/MS, following in-gel digestion with trypsin. The spots representing identified proteins are indicated in Fig. 1D and are designated with their ID accession numbers of Swiss Prot database. Score relates to the probability assignment. Score and sequence coverage were calculated by MASCOT search engine (http://www.matrixscience.com).

Table 2
Functions regulated by proteins that showed an altered expression in $APPE_{693\Delta}$-transgenic mouse hippocampus.

Function	Identified protein	Up/down
Cytoskeletal and their interacting proteins	Neurofilament light polypeptide	Down
	Alpha-internexin	Down
	Actin, cytoplasmic 1	Up/down
	Tubulin β-2A Chain	Up
Chaperone and their interacting proteins	Stress-induced-phosphoprotein 1	Down
	60 kDa heat shock protein	Down
	Heat shock cognate 71 kDa protein	Down
Energy metabolic proteins	Alpha-enolase	Down
	Gamma-enolase	Up
	ATP synthase subunit beta	Up
Vesicle transport and recycling	Dynamin-1	Up
	Clathrin light chain B	Up
Signaling proteins	Protein kinase C and casein kinase substrate in neurons protein 1	Down

The analysis of proteins function was done by using MOTIF (http://www.genome.jp/tools/motif/).

[12]. The amount of dynamin was significantly increased. Our findings in $APP_{E693\Delta}$-transgenic mice without plaque deposition are consistent with previous findings that protein levels of dynamin were increased in Tg2576 mice with plaque deposition [21], suggesting that the release of neurotransmitter is affected by dynamin increased irrespective of AD stage. Also, spot no. 6 was identified as Pacsin 1. The Pacsin 1 is colocalized, oligomerized and bound with dynamin, and both proteins participate in synaptic vesicle endocytosis [17]. The amount of Pacsin 1 was significantly increased. Taken together, Pacsin 1 and dynamin enhanced by Aβ oligomers

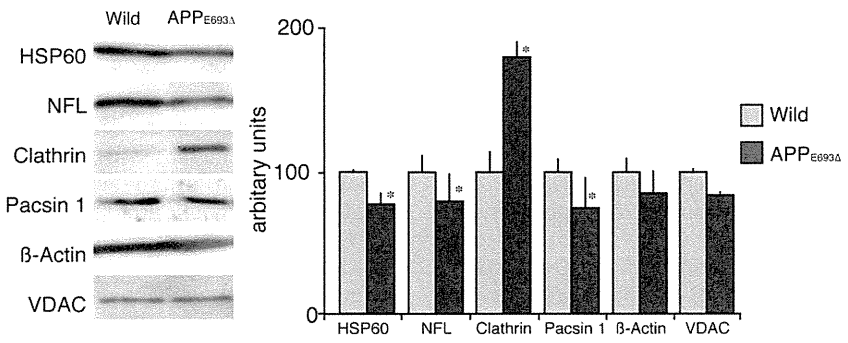

Fig. 2. Differentially expressed proteins validated by Western blotting for the hippocampus of non-transgenic and $APP_{E693\Delta}$-transgenic mice. (A) The levels of HSP60, NFL, clathrin, Pacsin 1, β-actin and VDAC in individual samples of each group were detected. (B) Graphical representation of the semi quantitative analysis (mean ± SEM of O.D. of bands). Data are presented as mean ± SEM ($n = 4$) *t*-test; $^*P < 0.05$ vs. $APP_{E693\Delta}$-transgenic mice.

might change the function of synaptic vesicle in the hippocampus of AD.

Spot no. 18 was identified as clathrin, which is known as the major protein of the polyhedral coat of coated pits and vesicles [7]. The amount of spot no. 18 was significantly decreased. APP was associated clusters of clathrin-coated vesicles and endosomes [3]. Thus, Aβ oligomers might inhibit the vesicle formation by clathrin.

In addition, we performed a validation experiment for HSP60, NFL, clathrin, Pacsin 1 and β-actin as the altered proteins, and VDAC as the unchanged protein (as control) [23]. The increased levels of clathrin, the decreased levels of HSP60, NFL, and Pacsin 1 and the unchanged level of β-actin and VDAC in $APP_{E693\Delta}$-transgenic mice hippocampus were validated by Western blotting (Fig. 2).

In summary, we identified the altered levels of 14 proteins in $APP_{E693\Delta}$-transgenic mice hippocampus using 2D-DIGE and LC–MS/MS approach. This approach elucidated the pathological effects of Aβ oligomers on hippocampus. Our findings might provide a clue for investigation of the hippocampus of AD early stage.

Acknowledgements

This work was supported by grants from Kobe Gakuin University for Collaborative Research C and the Smoking Research Foundation. The authors thank Dr. Tadanori Mayumi for his encouragement during the early days of the study.

References

[1] U. Andersson, H. Antonicka, J. Houstek, B. Cannon, A novel principle for conferring selectivity to poly(A)-binding proteins: interdependence of two ATP synthase beta-subunit mRNA-binding proteins, Biochemical Journal 346 (Pt 1) (2000) 33–39.
[2] C.L. Chien, R.K. Liem, Characterization of the mouse gene encoding the neuronal intermediate filament protein alpha-internexin, Gene 149 (1994) 289–292.
[3] A. Ferreira, A. Caceres, K.S. Kosik, Intraneuronal compartments of the amyloid precursor protein, Journal of Neuroscience 13 (1993) 3112–3123.
[4] T.A. Fulga, I. Elson-Schwab, V. Khurana, M.L. Steinhilb, T.L. Spires, B.T. Hyman, M.B. Feany, Abnormal bundling and accumulation of F-actin mediates tau-induced neuronal degeneration in vivo, Nature Cell Biology 9 (2007) 139–148.
[5] A. Gorg, C. Obermaier, G. Boguth, A. Harder, B. Scheibe, R. Wildgruber, W. Weiss, The current state of two-dimensional electrophoresis with immobilized pH gradients, Electrophoresis 21 (2000) 1037–1053.
[6] J. Hardy, D.J. Selkoe, The amyloid hypothesis of Alzheimer's disease: progress and problems on the road to therapeutics, Science 297 (2002) 353–356.
[7] J. Hirst, M.S. Robinson, Clathrin and adaptors, Biochimica et Biophysica Acta 1404 (1998) 173–193.
[8] C.R. Hunt, A.J. Parsian, P.C. Goswami, C.A. Kozak, Characterization and expression of the mouse Hsc70 gene, Biochimica et Biophysica Acta 1444 (1999) 315–325.
[9] S. Ikawa, R.A. Weinberg, An interaction between p21ras and heat shock protein hsp60, a chaperonin, Proceedings of the National Academy of Sciences 89 (1992) 2012–2016.
[10] J.L. Johnson, A. Halas, G. Flom, Nucleotide-dependent interaction of Saccharomyces cerevisiae Hsp90 with the cochaperone proteins Sti1, Cpr6, and Sba1, Molecular and Cellular Biology 27 (2007) 768–776.
[11] M. Kaghad, X. Dumont, P. Chalon, J.M. Lelias, N. Lamande, M. Lucas, M. Lazar, D. Caput, Nucleotide sequences of cDNAs alpha and gamma enolase mRNAs from mouse brain, Nucleic Acids Research 18 (1990) 3638.
[12] B.L. Kelly, R. Vassar, A. Ferreira, Beta-amyloid-induced dynamin 1 depletion in hippocampal neurons. A potential mechanism for early cognitive decline in Alzheimer disease, Journal of Biological Chemistry 280 (2005) 31746–31753.
[13] W.L. Klein, G.A. Krafft, C.E. Finch, Targeting small Abeta oligomers: the solution to an Alzheimer's disease conundrum? Trends in Neurosciences 24 (2001) 219–224.
[14] T.B. Kuhn, P.J. Meberg, M.D. Brown, B.W. Bernstein, L.S. Minamide, J.R. Jensen, K. Okada, E.A. Soda, J.R. Bamburg, Regulating actin dynamics in neuronal growth cones by ADF/cofilin and rho family GTPases, Journal of Neurobiology 44 (2000) 126–144.
[15] V.M. Lee, M. Goedert, J.Q. Trojanowski, Neurodegenerative tauopathies, Annual Review of Neuroscience 24 (2001) 1121–1159.
[16] S. Li, S. Hong, N.E. Shepardson, D.M. Walsh, G.M. Shankar, D. Selkoe, Soluble oligomers of amyloid Beta protein facilitate hippocampal long-term depression by disrupting neuronal glutamate uptake, Neuron 62 (2009) 788–801.
[17] J. Modregger, B. Ritter, B. Witter, M. Paulsson, M. Plomann, All three PACSIN isoforms bind to endocytic proteins and inhibit endocytosis, Journal of Cell Science 113 (Pt 24) (2000) 4511–4521.
[18] R.A. Nixon, R.K. Sihag, Neurofilament phosphorylation: a new look at regulation and function, Trends in Neurosciences 14 (1991) 501–506.
[19] R.A. Robinson, M.B. Lange, R. Sultana, V. Galvan, J. Fombonne, O. Gorostiza, J. Zhang, G. Warrier, J. Cai, W.M. Pierce, D.E. Bredesen, D.A. Butterfield, Differential expression and redox proteomics analyses of an Alzheimer disease transgenic mouse model: effects of the amyloid-beta peptide of amyloid precursor protein, Neuroscience 177 (2011) 207–222.
[20] D.J. Selkoe, Alzheimer's disease is a synaptic failure, Science 298 (2002) 789–791.
[21] S.J. Shin, S.E. Lee, J.H. Boo, M. Kim, Y.D. Yoon, S.I. Kim, I. Mook-Jung, Profiling proteins related to amyloid deposited brain of Tg2576 mice, Proteomics 4 (2004) 3359–3368.
[22] R. Sultana, D. Boyd-Kimball, J. Cai, W.M. Pierce, J.B. Klein, M. Merchant, D.A. Butterfield, Proteomics analysis of the Alzheimer's disease hippocampal proteome, Journal of Alzheimer's Disease 11 (2007) 153–164.
[23] M. Takano, K. Maekura, M. Otani, K. Sano, T. Nakamura-Hirota, S. Tokuyama, K.S. Min, T. Tomiyama, H. Mori, S. Matsuyama, Proteomic analysis of the brain tissues from a transgenic mouse model of amyloid beta oligomers, Neurochemistry International 61 (2012) 347–355.
[24] M. Takano, M. Otani, A. Sakai, K. Kadoyama, S. Matsuyama, A. Matsumoto, M. Takenokuchi, M. Sumida, T. Taniguchi, Use of a phosphosensor dye in proteomic analysis of human mutant tau transgenic mice, Neuroreport 20 (2009) 1648–1653.
[25] T. Tomiyama, S. Matsuyama, H. Iso, T. Umeda, H. Takuma, K. Ohnishi, K. Ishibashi, R. Teraoka, N. Sakama, T. Yamashita, K. Nishitsuji, K. Ito, H. Shimada, M.P. Lambert, W.L. Klein, H. Mori, A mouse model of amyloid beta oligomers: their contribution to synaptic alteration, abnormal tau phosphorylation, glial activation, and neuronal loss in vivo, Journal of Neuroscience 30 (2010) 4845–4856.

—Review—

抗体工学を駆使した創薬ターゲットの探索技術

鎌田春彦

Exploring Technique for Pharmaceutical Target Using Antibody Technology

Haruhiko Kamada

Laboratory of Biopharmaceutical Research, National Institute of Biomedical Innovation; 7-6-8 Saito-Asagi, Ibaraki, Osaka 567-0085, Japan.

(Received December 2, 2011)

A monoclonal antibody (Mab), due to its specific binding ability to a target protein, can potentially be one of the most useful tools for the functional analysis of proteins in recent proteomics-based research. However, the production of Mab is a very time-consuming and laborious process (*i.e.*, preparation of recombinant antigens, immunization of animals, preparation of hybridomas), making it the rate-limiting step in using Mabs in high-throughput proteomics research, which heavily relies on comprehensive and rapid methods. Therefore, there is a great demand for new methods to efficiently generate Mabs against a group of proteins identified by proteome analysis. Here, we describe a useful method called "Antibody proteomic technique" for the rapid generations of Mabs to pharmaceutical target, which were identified by proteomic analyses of disease samples (ex. tumor tissue, *etc.*). We also introduce another method to find profitable targets on vasculature, which is called "Vascular proteomic technique". Our results suggest that this method for the rapid generation of Mabs to proteins may be very useful in proteomics-based research as well as in clinical applications.

Key words——monoclonal antibody; proteomics; biomarker; biologics

1. はじめに

近年，ゲノム解析やジーンチップ解析などのオミクス研究の進展に伴い，バイオマーカー探索や創薬のための標的分子の探索が盛んに行われている.[1,2] このような医薬品開発に資する標的分子の探索は，画期的な医薬品を開発する上で最も重要なステップであり，探索の結果から得られた標的分子に作用する薬物は，これまで治療法のなかった疾患の治療に貢献すると考えられている．このような疾患の発症や悪化の原因となる標的分子の探索のうち，とりわけプロテオミクスを用いたタンパク質の発現解析は注目を集めており，医薬品の開発に貢献するものと期待されている.[3] しかしながら，上述したオミクス解析全般に言えることであるが，標的分子の探索から創薬ターゲットの発見につながった例はこれまでほとんどないのが現状である．疾患の発症や悪化に連動して発現変化が認められる疾患関連分子は，病態時に数百以上のオーダーで発現変動しており，そのほとんどが疾患の発症や悪化には直接関係していないものであるとされている.[4] したがって，画期的診断法・治療法を開発していくためには，このような疾患関連分子の中から，創薬に資する分子を効率よく同定する必要があり，これまで用いられてきた方法をより進歩させた新しい探索法の開発に期待が寄せられている．

このように標的分子を検出したり薬理効果発現を評価したりするためには，標的分子を認識可能なプローブが必要であり，標的分子候補タンパク質に結合活性を持つ抗体の開発がますます重要視されつつある．特に，最近では抗体そのものを医薬品化した抗体医薬品がリウマチやがんなど様々な難治性疾患に臨床応用され，バイオ医薬品の市場規模が急拡大している.[5] これまでに臨床応用された抗体医薬品としては抗サイトカイン抗体などの活性中和抗体や細胞表面のマーカー分子を認識する抗細胞抗体がほ

独立行政法人医薬基盤研究所バイオ創薬プロジェクト（〒567-0085 大阪府茨木市彩都あさぎ 7-6-8）
e-mail: kamada@nibio.go.jp

本総説は，日本薬学会第 131 年会シンポジウム S16 で発表したものを中心に記述したものである．

とんどであるが，最近では受容体に結合して活性を示すアゴニスト抗体や2種類のマーカー分子を認識して活性を示すバイスペシフィック抗体なども臨床応用に向けた検討が進められつつある.[6]

このような抗体医薬は，従来の低分子医薬品や分子プローブでは困難な疾患に対する治療や診断が可能であるために，様々な難治性疾患の克服に向け大いに利用されつつあるところであるが，抗体医薬の開発を効率よく進めるためにはいくつかの問題点があることが知られている．その1つの問題点として，一般的に1種類の抗体の作製期間は，数ヵ月程度必要とされ，このことが原因となって標的分子が同定されてからその評価までには大きなタイムラグが生じており，タンパク質の中からスクリーニングする上での障害となっていることが指摘されている.

もし数多くの発現変動タンパク質に対する特異的抗体が一挙かつ迅速に作製できれば，定量解析（ELISA, Western blot (WB), *etc.*），局在解析（免疫染色，WB, *etc.*），機能解析（細胞増殖活性，細胞分化解析，*etc.*）が可能になり，タンパク質の発現挙動と疾患の発症・悪化などとの連関解析が格段に進展するものと考えられる．そこでわれわれは，プロテオーム解析技術の最適化とともに，数多くの変動タンパク質の中から，創薬に向けて標的分子を絞り込む基盤技術の開発を行うために，プロテオミクスと抗体工学を融合させた新しい「抗体プロテオミクス技術」を開発した．本総説では，この「抗体プロテオミクス技術」を概説し創薬ターゲット候補分子の同定に至った例を示すとともに，抗体をバイオ医薬品として利用する際に有用な探索技術として「血管プロテオミクス」に関してもその研究成果を一部紹介する.

2. 抗体プロテオミクス技術

抗体は生体内で外来異物由来のタンパク質抗原を認識し，それを捕捉するための生体防御分子としての役割を持っている．すなわち，あらゆる外来抗原に対して，結合可能なレパートリーを有するタンパク分子群である．その性質を利用し，古くからタンパク質の定性や定量のためのツールとして，生命科学の分野で活用されている．われわれは，この抗体の持つ性質に着目し，生体の抗体レパートリーを再現した抗体ライブラリを手に持つことで，抗原に結合可能な抗体分子を短時間で手に入れたいと考えた．この膨大な抗体ライブラリの中から目的の抗体を迅速に単離するための基盤技術としてわれわれはファージ抗体ライブラリに着目した．このファージ抗体ライブラリは，抗体の抗原認識部位にあたるV領域をリンカーで結んだ一本鎖抗体（scFV 抗体）をファージの外殻タンパク質gⅢとの融合タンパク質としてファージ表面に提示しており，ファージウイルスの表面に提示させた一本鎖抗体をライブラリとして作製することが可能である.[7] この技術は，一般的に用いられるハイブリドーマ法とは異なり，*in vitro* のセレクションのみで迅速にモノクローナル抗体を単離することができ，2週間程度の短期間でモノクローナル抗体が得られる方法である．この技術を従来から知られる二次元電気泳動法などを利用したプロテオミクス技術と組み合わせ，単離・精製したタンパク質に対して上述した抗体ライブラリからの抗体の単離を行おうと考えた．さらに得られた抗体を利用し，免疫染色を利用した抗原の発現解析を組織マイクロアレイを用いて迅速に行うことにした．この組織マイクロアレイは，がんなどの疾患組織が直径1–2 mm 程度の組織片として添付されたスライドガラスであり，一挙に100症例以上もの組織を免疫染色などで検出することが可能である.[8] この組織マイクロアレイを用いることで，これまで発現解析が困難であった組織を一挙に染色でき，極めて短時間にタンパク質の発現状態を知ることができる．この抗体ライブラリをプロテオミクス，さらに組織マイクロアレイと融合した「抗体プロテオミクス技術」をわれわれは独自に開発し，がんの標的分子の探索を行うことにした（Fig. 1）.[9]

まず，ナイーブファージ抗体ライブラリをウェスタンブロット等に用いられるメンブランに固相化した精製タンパク質に対してパンニングを行い，わずか10 ng 程度のモデル抗原からでもモノクローナル抗体を得ることができた．さらに，この方法を乳がんの診断・治療に応用し，画期的な標的分子の探索を行うために，正常乳腺とのタンパク質比較解析を行った．その結果，十数種類前後の標的分子候補の中から最も有用な創薬ターゲットとしてEphrin Receptor A10（EphA10）と呼ばれる分子を同定した（Table 1）．この分子は，乳がん細胞に特異的に発現する上，既存の乳がんの標的分子として知られるHer-2よりも高い陽性率を示し，Her-2陰性患者

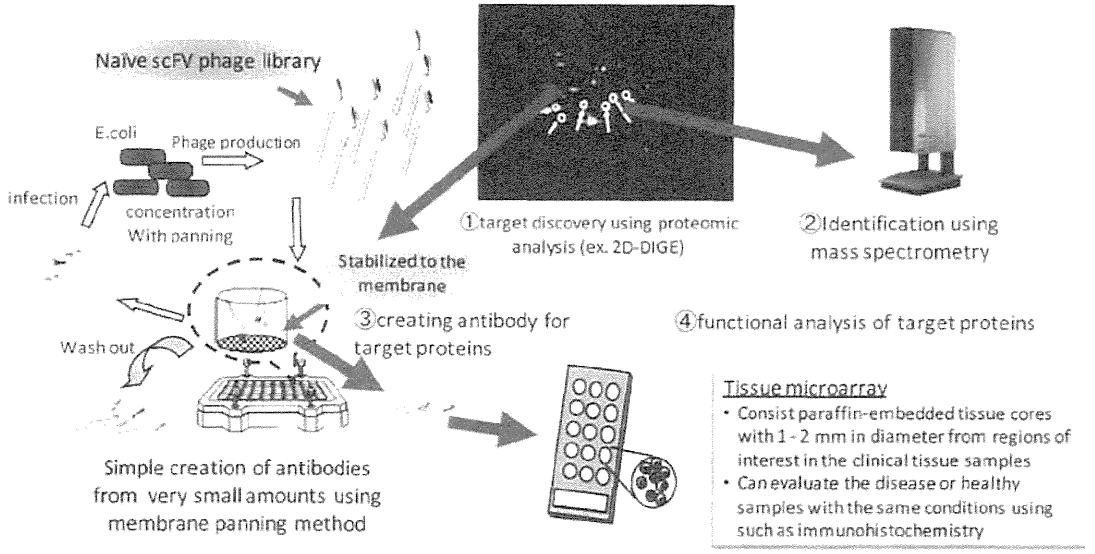

Fig. 1. Schematic Protocol of Antibody Proteomics

Table 1. Protein Expression of Identified Drug Target Candidates Using Tissue Microarray

Target candidate	Positive ratio	
	Healthy mammal	Breast cancer
Her2 (Control)	0/15(0%)	53/189(28%)
IkappaBR	3/15(20%)	22/189(12%)
SPATA5 protein	0/15(0%)	0/189(0%)
beta actin variant	0/15(0%)	0/189(0%)
TRAIL-R2	0/15(0%)	119/189(63%)
RREB-1	1/15(6%)	83/189(44%)
FLJ31438 protein	0/15(0%)	0/189(0%)
hPAK65	0/15(0%)	0/189(0%)
Cytokeratin 8	0/15(0%)	137/189(73%)
XRN1 protein	0/15(0%)	0/189(0%)
Jerky protein homolog-like	0/15(0%)	0/189(0%)
EPH receptor A10 (EphA10)	0/15(0%)	93/189(49%)

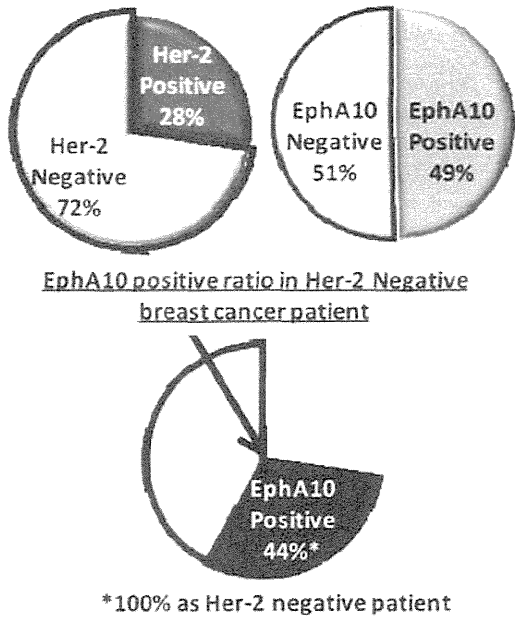

Fig. 2. EphA10 Expression in Breast Cancer Patients

の約半数に発現する創薬ターゲットとしても有用性の高い分子であることが明らかになった（Fig. 2）.

3. 血管プロテオミクス

このように創薬ターゲットとしての分子探索にプロテオミクスの手法を用いることは極めて有用であり，今後数多くの標的分子を発見できる可能性を示唆している．その一方で，現在の抗体医薬の標的分子のほとんどが，膜タンパク質及び分泌タンパク質を標的とした分子標的治療薬である事実からも，抗体医薬を用いる限り，現在の技術背景では，細胞質内に存在するタンパク質を標的にするのは数多くの問題点があると考えられている.[10] したがって，抗体医薬の開発を念頭に置く場合には，膜タンパク質や分泌タンパク質を標的にすることが実用化において最も近道であると考えられる．そこで，細胞膜タンパク質，及び細胞外マトリクス等の分泌タンパク質の発現挙動の解析のために，全身の血管をビオチン化試薬にてラベル化し，疾患組織にある血管内皮

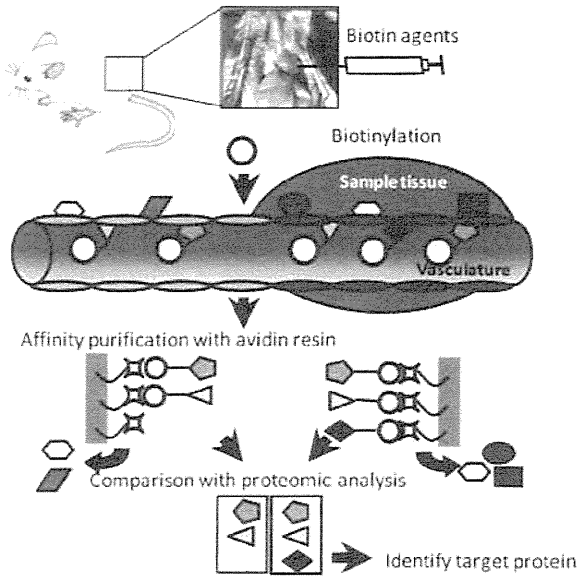

Fig. 3. Schematic Protocol of Vasculature Proteomics

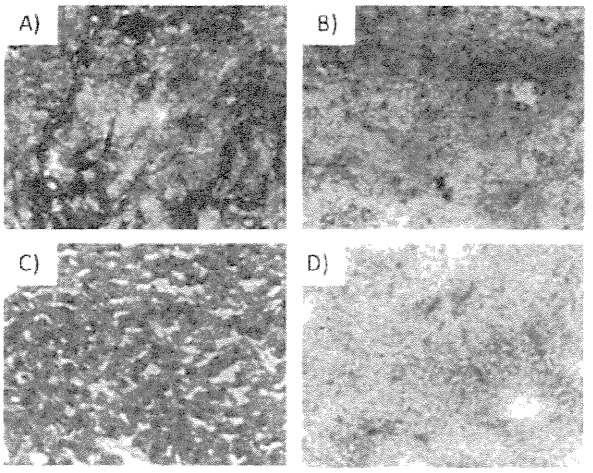

Fig. 4. BST-2 Expression in Metastatic Lymphoma
(A) Liver metastatic tumor; (B) Spleen metastatic tumor; (C) Normal liver; (D) Normal spleen. Immunohistochemistry were performed by using anti-BST-2 polyclonal antibody. Tumor vascular regions were stained (dark gray) but not normal tissues.

細胞の膜タンパク質並びに分泌タンパク質を効率よく回収・精製可能な *in vivo* biotinylation 法を活用し血管プロテオームを行うことにした.[11] Figure 3 にその概要を示す. この *in vivo* biotinylation 法は, 細胞膜タンパク質を解析する場合に, 現在汎用されている組織抽出後の膜タンパク質を回収する方法とは異なり, 直接組織細胞の外側からラベル化を行うため, 小胞膜のコンタミネーションのリスクを回避できる. 当然のことながら, 細胞外の膜タンパク質等を選択的にビオチンラベルするため, 解析結果から得られたタンパク質候補に対するモノクローナル抗体は, 通常の方法でプロテオーム解析して得られたタンパク質候補（多くの場合, シャペロンタンパク質やヒートショックタンパク質といった細胞内タンパク質）に対する抗体よりも, 基礎医学・臨床医学的な有用性に優れていることは言うまでもない. そのうえ, 血管側からビオチン化しているため, 組織中の血管内皮細胞がより効率よくラベル化されており, 抗体医薬の開発には極めて有用な方法であると考えられる.

この血管プロテオミクスを担がんマウスモデルに対して行い, 転移性リンパ腫の治療に向けた抗原の探索を行った.[12] 具体的には, 抗体のラベル化等に用いるビオチン化試薬を, *in vivo* に直接投与・環流することで, 組織に存在する血管を直接ラベル化した. その結果, 腫瘍血管での発現がこれまでにも報告されている Transferrin 受容体が同定された一方, これまで知られていなかった新しいがん血管関連抗原として BST-2 の発現を見い出した（Fig. 4）.[12] BST-2 は, 肝臓や脾臓に転移したリンパ腫の血管部位に特異的に発現しており, これを標的としたがん治療薬の開発が期待される. 実際に, この BST-2 に対する抗体を投与することで, 腫瘍の増殖が抑制される結果も見い出しており, 今後これらを利用した抗体医薬の開発も期待されるところである.

4. 結論と展望

抗体プロテオミクス技術はプロテオミクスと抗体工学の技術を組み合わせ, さらに組織マイクロアレイによるバリデーションを迅速に行うことで, 標的分子を迅速にバリデーションできる技術である. この技術により, これまで標的分子の探索から発現解析までの膨大な時間と労力を, わずか 2–3 週間程度の期間で達成できる極めて有用な技術として開発することができた. また先述したように血管プロテオミクスは, 個体レベルでのプロテオミクスを可能とするうえ, 細胞膜タンパク質及び細胞外マトリクス等の分泌タンパク質を効果的にラベル化できる方法であり, 細胞質内タンパク質のコンタミネーションを回避できるという圧倒的な利点を有している. この 2 つのプロテオミクス技術を融合することで, 疾患における創薬ターゲットの同定に留まらず, 新しい抗体医薬の開発法として利用することを考えてい

る．今後，本方法を用いて同定された抗原に対する抗体を作製することで，バイオマーカーの検出や評価に利用できるものと期待されるとともに，タンパク質の発現挙動解析，並びに同定作業を現在も進めているところであり，プロテオミクスによる解析基盤の確立に向けた開発・最適化を今後も行う予定である．

謝辞　本研究は，多くの共同研究者の先生方に御支援を賜りつつ，大阪大学薬学研究科毒性学分野及び医薬基盤研究所バイオ創薬プロジェクトのスタッフ・学生の皆さんとともに推進したものです．この場をお借りして，心より御礼を申し上げます．さらに，プロテオーム解析にあたり医薬基盤研究所免疫シグナルプロジェクト 世良田 聡先生，仲 哲治先生にご協力頂くとともに，血管プロテオミクスに関しては，スイス連邦工科大学チューリッヒ校(ETHZ)のダリオ・ネリ教授のご協力を得ました．また本研究の推進にあたり，厚生労働科学研究費補助金並びに文部科学研究費補助金の支援を賜りました．ここに深謝申し上げます．

REFERENCES

1) Kramer R., Cohen D., *Nat. Rev. Drug Discov.*, **3**, 965–972 (2004).
2) Butte A., *Nat. Rev. Drug Discov.*, **1**, 951–960 (2002).
3) Latterich M., Schnitzer J. E., *Nat. Biotechnol.*, **29**, 600–602 (2011).
4) Rifai N., Gillette M. A., Carr S. A., *Nat. Biotechnol.*, **24**, 971–983 (2006).
5) Goodman M., *Nat. Rev. Drug Discov.*, **8**, 837 (2009).
6) Nelson A. L., Reichert J. M., *Nat. Biotechnol.*, **27**, 331–337 (2009).
7) Yamashita T., Utoguchi N., Suzuki R., Nagano K., Tsunoda S., Tsutsumi Y., Maruyama K., *Yakugaku Zasshi*, **130**, 479–485 (2010).
8) Giltnane J. M., Rimm D. L., *Nat. Clin. Pract. Oncol.*, **1**, 104–111 (2004).
9) Imai S., Nagano K., Yoshida Y., Okamura T., Yamashita T., Abe Y., Yoshikawa T., Yoshioka Y., Kamada H., Mukai Y., Nakagawa S., Tsutsumi Y., Tsunoda S., *Biomaterials*, **32**, 162–169 (2011).
10) Williams B. R., Zhu Z., *Curr. Med. Chem.*, **13**, 1473–1480 (2006).
11) Roesli C., Neri D., *J. Proteomics*, **73**, 2219–2229 (2010).
12) Schliemann C., Roesli C., Kamada H., Borgia B., Fugmann T., Klapper W., Neri D., *Blood*, **115**, 736–744 (2010).

The δ2 glutamate receptor gates long-term depression by coordinating interactions between two AMPA receptor phosphorylation sites

Kazuhisa Kohda[a,b,1], Wataru Kakegawa[a,b,1], Shinji Matsuda[a,b,c], Tadashi Yamamoto[d], Hisashi Hirano[e], and Michisuke Yuzaki[a,b,2]

[a]Department of Physiology, School of Medicine, Keio University, Shinjuku-ku, Tokyo 160-8582, Japan; [b]Core Research for Evolutional Science and Technology (CREST) and [c]Precursory Research for Embryonic Science and Technology (PREST), Japan Science and Technology Agency, Kawaguchi, Saitama 332-0012, Japan; [d]Cell Signal Unit, Okinawa Institute of Science and Technology Graduate University, Kunigami, Okinawa 904-0495, Japan; and [e]Division of Functional Proteomics, Yokohama City University, Turumi-ku, Yokohama 230-0045, Japan

Edited* by Masao Ito, RIKEN Brain Science Institute, Wako, Japan, and approved January 24, 2013 (received for review October 23, 2012)

Long-term depression (LTD) commonly affects learning and memory in various brain regions. Although cerebellar LTD absolutely requires the δ2 glutamate receptor (GluD2) that is expressed in Purkinje cells, LTD in other brain regions does not; why and how cerebellar LTD is regulated by GluD2 remains unelucidated. Here, we show that the activity-dependent phosphorylation of serine 880 (S880) in GluA2 AMPA receptor subunit, which is an essential step for AMPA receptor endocytosis during LTD induction, was impaired in *GluD2*-null cerebellum. In contrast, the basal phosphorylation levels of tyrosine 876 (Y876) in GluA2 were increased in *GluD2*-null cerebellum. An in vitro phosphorylation assay revealed that Y876 phosphorylation inhibited subsequent S880 phosphorylation. Conversely, Y876 dephosphorylation was sufficient to restore S880 phosphorylation and LTD induction in *GluD2*-null Purkinje cells. Furthermore, megakaryocyte protein tyrosine phosphatase (PTPMEG), which binds to the C terminus of GluD2, directly dephosphorylated Y876. These data indicate that GluD2 gates LTD by coordinating interactions between the two phosphorylation sites of the GluA2.

synaptic plasticity | mouse

Synaptic plasticity, such as long-term potentiation and long-term depression (LTD), is believed to underlie learning and memory processes in vivo. LTD is observed in various brain regions, including the cerebellum and hippocampus, and it is commonly caused by clathrin-dependent endocytosis of postsynaptic AMPA-type glutamate receptors. However, cerebellar LTD is unique, because it requires the presence of another class of glutamate receptors, the δ2 glutamate receptor (GluD2) (1), which is predominantly expressed in parallel fiber (PF)–Purkinje cell synapses. *GluD2*-null mice display ataxia and impaired motor learning (2). GluD2 does not normally function as an ion channel; instead, its C-terminal end, which constitutes a postsynaptic density-95/discs-large/zonula occludens-1 (PDZ) ligand domain, is essential for LTD induction. LTD is abolished in WT Purkinje cells that have been acutely perfused with a short peptide that corresponds to the PDZ ligand domain of GluD2 (3). Although morphological abnormalities in *GluD2*-null cerebellum are rescued by the expression of a mutant GluD2 transgene that lacks the PDZ ligand domain, LTD and motor learning remain impaired (4). These results indicate that the C terminus of GluD2, to which several PDZ proteins, such as PSD-93, megakaryocyte protein tyrosine phosphatase (PTPMEG), S-SCAM, n-PIST, and delphilin, bind (5), plays a crucial role in LTD induction and motor learning. However, an answer to the fundamental question of how GluD2 regulates cerebellar LTD remains unelucidated.

AMPA receptor endocytosis is generally regulated by changes in the phosphorylation status of AMPA receptor subunits. The activity-dependent phosphorylation of serine 880 (S880) in the GluA2 subunit plays an important role in AMPA receptor endocytosis and LTD induction through the release of glutamate receptor interacting protein 1, which is an anchoring protein, from the C terminus of the AMPA receptors at both hippocampal (6, 7) and cerebellar synapses (8–10). However, how this process is regulated and how it mediates LTD is not completely understood. In addition to the phosphorylation of S880, the phosphorylation of tyrosine 876 (Y876) in the GluA2 subunit regulates AMPA receptor endocytosis during metabotropic glutamate receptor (mGluR) -dependent LTD at hippocampal synapses (11–14). However, whether Y876 phosphorylation is involved in cerebellar LTD, which is dependent on mGluR1, is unknown. In addition, its relationship with S880 phosphorylation is unclear.

In this study, we show that the activity-dependent phosphorylation of S880 in GluA2 was impaired in *GluD2*-null cerebellum. In contrast, the basal phosphorylation levels of Y876 in GluA2 were increased in *GluD2*-null cerebellum. Y876 phosphorylation inhibited subsequent S880 phosphorylation. Conversely, Y876 dephosphorylation restored S880 phosphorylation and LTD induction in *GluD2*-null Purkinje cells. Furthermore, interactions with the tyrosine phosphatase PTPMEG (15) at the C terminus of GluD2 were necessary and sufficient for GluD2 to regulate LTD induction. These results indicated that GluD2 serves as a master switch to gate inducibility of LTD by coordinating interactions between the two phosphorylation sites in GluA2 through its interaction with PTPMEG. Because PTPMEG and GluD1, which is a protein in the GluD2 family, are expressed in regions outside the cerebellum, similar regula-

Significance

Long-term depression (LTD) commonly affects learning and memory in various brain regions. Although LTD in the cerebellum absolutely requires δ2 glutamate receptors, its underlying mechanisms remain elusive. LTD is caused by endocytosis of AMPA receptors, which is triggered by activity-induced serine phosphorylation of the GluA2 subunit. Our work showed that this serine phosphorylation required prior dephosphorylation of the nearby tyrosine residue. By interaction with a tyrosine phosphatase, δ2 glutamate receptors regulated tyrosine dephosphorylation status of GluA2 to gate inducibility of LTD. These findings will provide better understanding of general mechanisms regulating AMPA receptor endocytosis during synaptic plasticity.

Author contributions: K.K., W.K., and M.Y. designed research; K.K. and W.K. performed research; S.M., T.Y., and H.H. contributed new reagents/analytic tools; K.K. and W.K. analyzed data; and K.K. and M.Y. wrote the paper.

The authors declare no conflict of interest.

*This Direct Submission article had a prearranged editor.

[1]K.K. and W.K. contributed equally to this work.

[2]To whom correspondence should be addressed. E-mail: myuzaki@a5.keio.jp.

This article contains supporting information online at www.pnas.org/lookup/suppl/doi:10.1073/pnas.1218380110/-/DCSupplemental.

tory mechanisms of AMPA receptor endocytosis may be operational in other brain regions.

Results

Increased Basal Phosphorylation Levels of Tyrosine in *GluD2*-Null Purkinje Cells. The phosphorylation of S880 (6–10) or Y876 (11, 12, 14, 16) in GluA2 (Fig. 1*A*) has been proposed to play important roles in AMPA receptor endocytosis and LTD. Thus, we first examined the basal phosphorylation of GluA2 in the synaptosomal fraction of cerebellar tissue from postnatal days (P) 21–30 WT and *GluD2*-null mice. An immunoblot analysis with phosphorylation-specific antibodies revealed weak basal phosphorylation of S880 and Y876 in GluA2 in WT cerebellum (Fig. 1*B* and Fig. S8). Basal phosphorylation levels of S880 in GluA2 were similar in WT and *GluD2*-null cerebellum (0.77 ± 0.19-fold vs. WT, $n = 7$ each, $P = 0.15$). Basal phosphorylation levels of Y876 in GluA2 were significantly increased in *GluD2*-null cerebellum compared with those levels in WT cerebellum (1.29 ± 0.11-fold vs. WT, $n = 11$ each, $P = 0.02$) (Fig. 1*B*). Thus, the loss of GluD2 from PF–Purkinje cell synapses increased the tyrosine phosphorylation levels of GluA2 in the cerebellum.

To clarify whether the increased phosphorylation levels of Y876 in GluA2 that were observed in the immunoblot analyses (Fig. 1*B*) reflected changes in the PF synapses of Purkinje cells, we examined PF-evoked slow excitatory postsynaptic currents ($_{slow}$EPSCs), which are activated by mGluR1 and regulated by the tyrosine phosphorylation levels of Purkinje cells (Fig. 1*A*) (17). We performed patch-clamp recordings in acutely prepared slices from P21–P35 mice and adjusted the PF stimulus intensity to evoke similar amplitudes of fast EPSCs, which are mediated by AMPA receptors ($_{AMPA}$EPSCs), between WT and *GluD2*-null Purkinje cells. Then, to evoke and isolate $_{slow}$EPSCs, tetanic stimulation (2–10 pulses at 100 Hz) was applied to PFs in the presence of the AMPA receptor antagonist NBQX. We observed that the amplitudes (Fig. 1*C*) and transferred charges of $_{slow}$EPSCs, which were normalized by transferred charges of $_{AMPA}$EPSCs, were significantly smaller in *GluD2*-null cells than those values in WT Purkinje cells (Fig. 1*C*) ($P = 0.001$ for amplitudes and $P = 0.006$ for transferred charges). PF-evoked $_{slow}$EPSCs were activated by mGluR1, which is coupled to the opening of the canonical transient receptor potential channel 1 (TRPC1) or TRPC3 (Fig. 1*A*) (18, 19). However, the immunohistochemical and immunoblot analyses did not show any decreases in the expression levels of mGluR1, TRPC1, or TRPC3 between WT and *GluD2*-null Purkinje cells (Fig. S1). Indeed, the functions of mGluR1 itself have been reported as normal in *GluD2*-null Purkinje cells (20). These data suggested that the phosphorylation levels of tyrosine were increased in *GluD2*-null Purkinje cells.

To further test this hypothesis, we reduced the tyrosine phosphorylation levels in WT and *GluD2*-null Purkinje cells by introducing 4-amino-1-*tert*-butyl-3-(1′-naphthyl)pyrazolo[3,4-d] pyrimidine (a PP1 analog; 10 μM for 20 min), which is a specific Src family tyrosine kinase (SFK) inhibitor, using a patch pipette. As

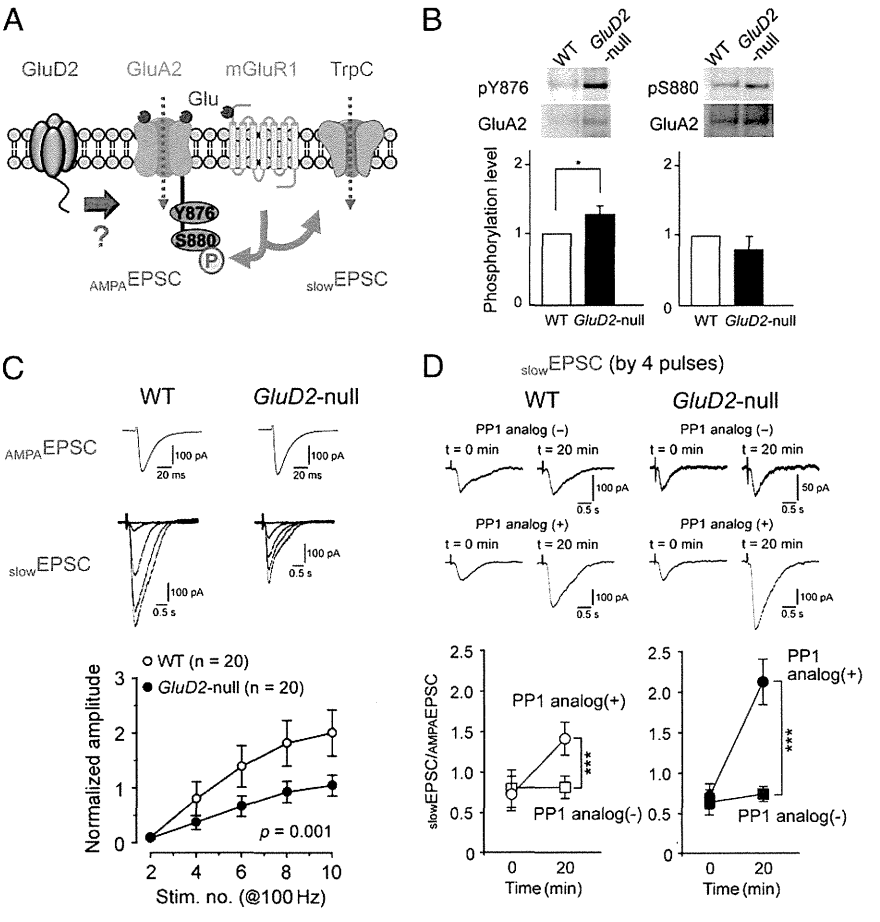

Fig. 1. Increased tyrosine phosphorylation in *GluD2*-null mice. (*A*) A schematic diagram illustrating the positions of Y876 and S880 at the C terminus of GluA2. LTD-inducing stimulation activates the mGluR1 and PKC to phosphorylate S880, which is an essential step for AMPA receptor endocytosis during LTD. mGluR1 activation also induces $_{slow}$EPSCs through the transient receptor potential channel (TRPC). In this paper, we have discussed whether and how GluD2 regulates these processes. (*B*) Basal-state phosphorylation of Y876 and S880 of GluA2 subunits of AMPA receptors in *GluD2*-null mice. Representative immunoblot images of the synaptosomal fraction of WT and *GluD2*-null cerebellum using an antibody against phosphorylated Y876 (pY876) or S880 (pS880) are shown in *Upper*. *Lower* shows intensities of pY876 (*Left*) or pS880 (*Right*) bands in *GluD2*-null cerebellum normalized by intensities of pY876 or pS880 bands in WT cerebellum. Basal-state phosphorylation of Y876, but not S880, was significantly increased in *GluD2*-null cerebellum. The bar represents mean and SEM. $*P < 0.05$ ($n = 11$ for Y876; $n = 7$ for S880). (*C*) Reduced $_{slow}$EPSC amplitudes in *GluD2*-null Purkinje cells. By adjusting PF stimulus intensities, similar sizes of PF-evoked $_{AMPA}$EPSCs were obtained in *GluD2*-null and WT Purkinje cells (*Top*). Then, PFs were stimulated 2–10 times at 100 Hz in the presence of AMPA receptor blockers to evoke $_{slow}$EPSCs (*Middle*). Amplitudes of $_{slow}$EPSCs were normalized by amplitudes of $_{AMPA}$EPSCs and plotted against the number of stimulations in *Bottom*. The bar represents mean and SEM. $P = 0.001$ ($n = 20$ each). (*D*) $_{slow}$EPSC amplitudes are enhanced by an SFK inhibitor PP1 analog in both WT and *GluD2*-null Purkinje cells. PFs were stimulated four times at 100 Hz in the presence of AMPA receptor blockers to evoke $_{slow}$EPSCs. When a PP1 analog was not included in the patch pipette [*Top*; PP1 analog (–)], there were no changes in amplitudes of $_{slow}$EPSCs between 0 and 20 min, whereas when a PP1 analog was included (*Middle*; +), amplitudes of $_{slow}$EPSCs at 20 min were significantly increased in both WT and *GluD2*-null Purkinje cells. *Lower* shows potentiating effects by a PP1 analog on $_{slow}$EPSC amplitudes, which were normalized by amplitudes of $_{AMPA}$EPSCs, in WT and *GluD2*-null Purkinje cells. The bar represents mean and SEM. $***P < 0.005$ ($n = 11$ for each group).

reported previously (17), $_{slow}$EPSCs that are evoked by a submaximal tetanus stimulus (four pulses at 100 Hz) to PFs significantly increased in response to the intracellular loading of a PP1 analog into WT Purkinje cells (Fig. 1 *C* and *D*). The reduced $_{slow}$EPSC amplitudes in *GluD2*-null Purkinje cells were rescued by treatment with the PP1 analog (Fig. 1 *C* and *D*). The PP1 analog exerted stronger enhancing effects on the $_{slow}$EPSC amplitudes in *GluD2*-null cells than the WT Purkinje cells; this finding may reflect higher basal tyrosine phosphorylation levels in *GluD2*-null Purkinje cells. These results indicated that the phosphorylation levels of tyrosine (including Y876 in GluA2) were generally increased at postsynaptic sites of PF–Purkinje cell synapses in *GluD2*-null cerebellum.

Activity-Dependent Increases in Y876 Phosphorylation Inhibited Activity-Induced S880 Phosphorylation in *GluD2*-Null Purkinje Cells. To biochemically determine the changes in the phosphorylation state of GluA2 during cerebellar LTD, we used a chemical LTD protocol, which involved a combination of 50 mM K^+ and 10 μM L-glutamate (K-glu), to mimic the climbing fiber-evoked depolarization of Purkinje cells and PF-induced activation (21). Cell lysates from WT and *GluD2*-null cerebellar slices that were treated with K-glu for 5 min were subjected to immunoblot analyses with phosphorylation-specific antibodies. We confirmed that S880 phosphorylation had significantly increased with K-glu treatment in WT cerebellum (1.84 ± 0.44-fold vs. no treatment control, $n = 8$ each, $P = 0.04$) (Fig. 2*A*), as reported previously (21). In contrast, K-glu treatment failed to induce S880 phosphorylation in *GluD2*-null cerebellum (1.15 ± 0.16-fold vs. control, $n = 13$ each, $P = 0.56$) (Fig. 2*B*). These data supported the concept that the phosphorylation of S880 in GluA2 was essential for cerebellar LTD (8, 10) and indicated that this step was impaired in *GluD2*-null cerebellum.

Although the rapid dephosphorylation of GluA2 tyrosine (12, 22), particularly at Y876 (14), has been reported in mGluR-dependent LTD in the hippocampus, whether Y876 phosphorylation is involved in cerebellar LTD has been unclear. We found that K-glu treatment significantly decreased the phosphorylation levels of Y876 in WT cerebellum (0.58 ± 0.12-fold vs. control, $n =$

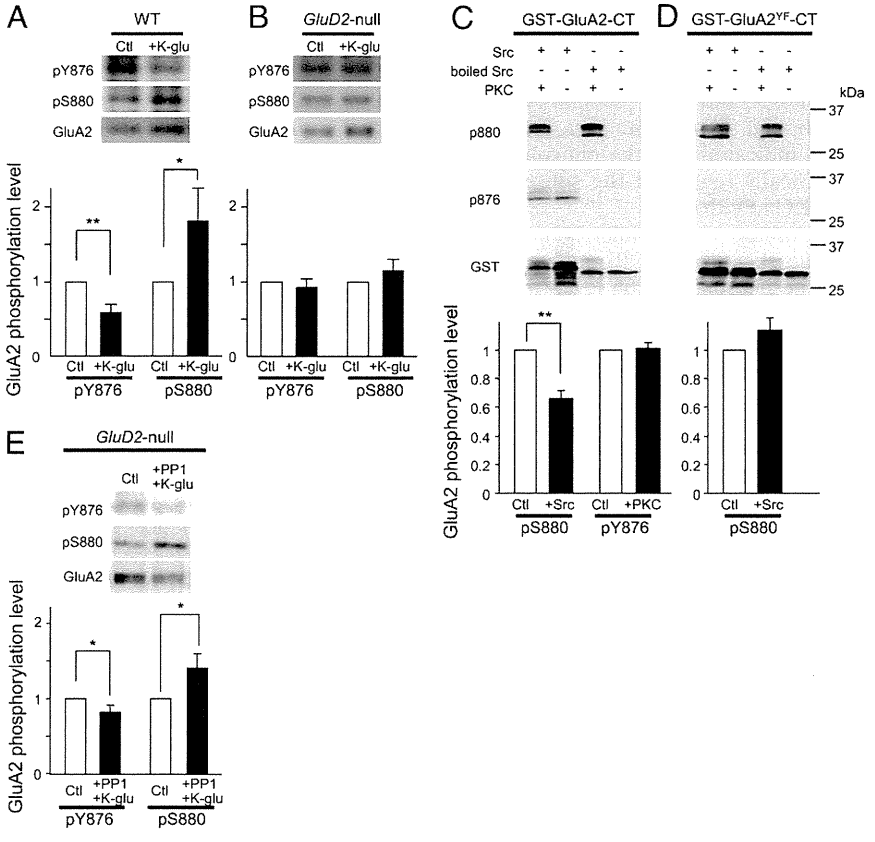

Fig. 2. Increased Y876 phosphorylation inhibits S880 phosphorylation. (*A* and *B*) Chemical LTD stimulus decreases Y876 phosphorylation but increases S880 phosphorylation in WT cerebellum (*A*), whereas it induces no changes at both sites in *GluD2*-null cerebellum (*B*). WT and *GluD2*-null cerebellar slices were treated with 50 mM KCl plus 10 μM L-glutamate for 5 min (K-glu), and the cell lysates were subjected to immunoblot analyses using phosphorylation-specific antibodies against Y876 (pY876) and S880 (pS880). Representative immunoblot images are shown in *Upper*. In *Lower*, intensities of pY876 and pS880 bands in K-glu–treated slices were normalized to those band intensities in untreated slices. The bar represents mean and SEM. $*P < 0.05$; $**P < 0.01$, respectively ($n = 8$ each for WT and $n = 13$ each for *GluD2*-null cerebellum). (*C* and *D*) Y876 phosphorylation inhibits subsequent S880 phosphorylation in the in vitro phosphorylation assay. The C-terminal region of GluA2 was conjugated with GST (GST-GluA2-CT). Y876 was replaced with phenylalanine to produce GST-GluA2^{YF}-CT. (*C*) GST-GluA2-CT or (*D*) GST-GluA2^{Y876F}-CT was incubated with Src or boiled Src followed by PKC. Phosphorylation of GluA2 was detected by antiphospho-Y876– and antiphospho-S880–specific antibodies. Representative immunoblot images are shown in *Upper*. The diagrams show intensities of S880 phosphorylation levels (pS880) with prior Src treatment (+Src) normalized by intensities of pS880 with boiled Src (Ctl). Intensities of Y876 phosphorylation levels (pY876) with subsequent PKC treatment (+PKC) normalized by intensities of pY876 without Src (Ctl) are also shown. The bar represents mean and SEM. $**P < 0.01$ ($n = 11$ for pY876 and $n = 13$ for pS880). (*E*) Inhibition of tyrosine phosphorylation restores K-glu–evoked changes in Y876 and S880 phosphorylation in *GluD2*-null cerebellum. Cerebellar slices from *GluD2*-null mice were preincubated with a PP1 analog for 15 min and then treated with K-glu in the presence of a PP1 analog. K-glu treatment significantly decreased Y876 phosphorylation and increased S880 phosphorylation in *GluD2*-null cerebellum. Representative immunoblot images are shown in *Upper*. In *Lower*, intensities of pY876 and pS880 bands in K-glu–treated slices were normalized to those band intensities in untreated slices. The bar represents mean and SEM. $*P < 0.05$ ($n = 16$ for pY876 and $n = 17$ for pS880).

8 each, $P < 0.01$) (Fig. 2*A*). K-glu treatment failed to induce changes in the phosphorylation levels of Y876 in *GluD2*-null cerebellar slices (0.93 ± 0.11-fold vs. control, $n = 13$ each, $P = 0.50$) (Fig. 2*B*). Thus, the basal phosphorylation levels of tyrosine had not only increased but also remained high after stimulation with K-glu in *GluD2*-null cerebellum.

Increased Y876 Phosphorylation Inhibited Activity-Induced S880 Phosphorylation in *GluD2*-Null Purkinje Cells. K-glu treatment failed to phosphorylate S880 and dephosphorylate Y876 in *GluD2*-null cerebellum. These two sites are located close to each other (Fig. 1*A*); therefore, we hypothesized that Y876 phosphorylation may interfere with subsequent S880 phosphorylation. To examine this hypothesis, we first performed an in vitro phosphorylation assay of the GluA2 C-terminal region that was fused to GST (GST-GluA2-CT). Immunoblot analyses with phosphorylation-specific antibodies confirmed that the GST-GluA2-CT was phosphorylated at Y876 and S880 in vitro by purified Src and PKC, respectively. Prior treatment of GST-GluA2-CT with Src, but not boiled Src, significantly decreased the subsequent S880 phosphorylation levels by PKC (0.66 ± 0.06-fold vs. boiled Src treatment, $n = 13$, $P < 0.001$), whereas the addition of PKC itself did not affect the phosphorylation levels of Y876 (Fig. 2*C*). In contrast, when Y876 was replaced with nonphosphorylatable phenylalanine (GST-GluA2^{Y876F}-CT), prior treatment with Src did not affect subsequent S880 phosphorylation by PKC (1.15 ± 0.13-fold vs. boiled Src treatment, $n = 6$, $P = 0.13$) (Fig. 2*D*). These results indicated that the phosphorylation of Y876 in GluA2 specifically regulated the subsequent phosphorylation of S880 by PKC in vitro.

To further examine this hypothesis in a cellular context, we pretreated *GluD2*-null cerebellar slices with a PP1 analog to reduce the increased basal tyrosine phosphorylation levels and examined whether K-glu treatment could induce S880 phosphorylation under such conditions. Immunoblot analyses confirmed that preincubation with the PP1 analog significantly reduced the basal phosphorylation levels of Y876 without affecting S880 phosphorylation in *GluD2*-null cerebellar slices (Fig. S2), indicating that basal Y876 phosphorylation levels were determined by the balance between endogenous SFK and phosphatase activities. As observed in WT cerebellar slices (Fig. 2*A*), subsequent K-glu treatment induced an increase in S880 phosphorylation levels (1.37 ± 0.19-fold vs. control, $n = 17$, $P = 0.04$) in *GluD2*-null cerebellar slices that had been pretreated with a PP1 analog (Fig. 2*E*). These results indicated that the increased basal phosphorylation of Y876 in GluA2 was responsible for the reduced S880 phosphorylation by K-glu in *GluD2*-null cerebellum.

Rescue of Impaired LTD in *GluD2*-Null Purkinje Cells by the Inhibition of the Phosphorylation of Y876 in GluA2. To establish the causal relationship between the increased Y876 phosphorylation levels and impaired LTD, we applied a PP1 analog to *GluD2*-null Purkinje cells using a patch pipette. The inclusion of a PP1 analog did not affect the baseline PF-evoked AMPA receptor-mediated EPSCs (PF-EPSCs) (Fig. S3) in WT and *GluD2*-null Purkinje cells. In addition, the application of conjunctive stimulation (CJ-stim; 30 cycles of PF stimulation plus Purkinje cell depolarization at 1 Hz) robustly induced LTD in WT Purkinje cells with (Fig. 3 *B* and *C*) (72 ± 5% at 25–30 min after CJ-stim, $n = 8$) or without a PP1 analog (Fig. 3 *A* and *C*) (74 ± 4% at 25–30 min after CJ-stim, $n = 9$, $P = 0.56$ vs. with a PP1 analog). In contrast, although CJ-stim failed to induce LTD in *GluD2*-null Purkinje cells (Fig. 3 *D* and *F*) (99 ± 2% at 25–30 min after CJ-stim, $n = 8$) as reported previously (2), it induced LTD in Purkinje cells with a PP1 analog (Fig. 3 *E* and *F*) (80 ± 5% at 25–30 min after CJ-stim, $n = 10$; $P = 0.006$ vs. without PP1 analog). These results indicated that impaired LTD in *GluD2*-null Purkinje cells was successfully rescued by the application of a PP1 analog to Purkinje cells and that increased tyrosine phosphorylation was responsible for the impaired LTD in *GluD2*-null Purkinje cells.

A PP1 analog could affect the tyrosine phosphorylation of many proteins in Purkinje cells. Thus, to examine the specific role of GluA2 phosphorylation at Y876 in LTD, we expressed GluA2 mutants, in which the tyrosine phosphorylation sites were disrupted, with a Sindbis virus vector in *GluD2*-null Purkinje cells. CJ-stim failed to induce LTD in *GluD2*-null Purkinje cells expressing WT GluA2 (Fig. 3 *G* and *J*) (89 ± 6% at 25–30 min after CJ-stim, $n = 6$) or mutant GluA2, in which phenylalanine replaced the two tyrosine residues at 869 and 873 (Fig. 3 *I* and *J*) (GluA2^{Y869F,Y873F}; 91 ± 6% at 25–30 min after CJ-stim, $n = 6$). In contrast, CJ-stim induced LTD in *GluD2*-null Purkinje cells expressing mutant GluA2, in which phenylalanine replaced the tyrosine at 876 (Fig. 3 *H* and *J*) (GluA2^{Y876F}; 66 ± 5% at 25–30 min after CJ-stim, $n = 5$, $P = 0.038$ vs. GluA2^{WT} and $P = 0.048$ vs. GluA2^{Y869F,Y873F}). Surface biotinylation assays showed that the cell surface expression levels of GluA2^{Y876F} and GluA2^{Y869F,Y873F} were comparable with the cell surface expression levels of WT GluA2 in human embryonic kidney 293 (HEK293) cells (Fig. S4). These results indicated that increased phosphorylation at Y876, but not at other tyrosine residues, at the C terminus of GluA2 was responsible for the impaired LTD, and its dephosphorylation was sufficient to restore LTD in *GluD2*-null mice.

Phosphorylation of Y876 Inhibited LTD Independent of the BRAG2-Arf6 Pathway in the Cerebellum. Recently, brefeldin-resistant Arf-guanine nucleotide exchange factor 2 (BRAG2), which activates Arf6, has been shown to bind to the C terminus of GluA2 in a manner that is dependent on Y876 dephosphorylation, and it, thereby, regulates AMPA receptor endocytosis at hippocampal synapses during LTD (14). Thus, the increased Y876 phosphorylation in *GluD2*-null Purkinje cells may inhibit the BRAG2-Arf6 pathway in addition to S880 phosphorylation. To examine this possibility, we used synthetic peptides that were derived from the C terminus sequence of GluA2 between positions 869 and 877 (^{869}**Y**KEG**Y**NV**Y**G^{877}) (Fig. 4*A*), which contained three tyrosine residues. The unphosphorylated peptides (pep-3Y), but not the unphosphorable peptides (pep-3A), in which alanine replaced the three tyrosine residues, have previously been shown to inhibit LTD induction in the amygdala (23), nucleus accumbens (24), and hippocampus (11, 14). In those studies, pep-3Y may have inhibited LTD induction by serving as a decoy peptide for BRAG2 (14) or a pseudosubstrate for SFKs (16). In contrast to the previous reports, the application of these peptides to WT Purkinje cells through a patch pipette did not affect CJ-stim–induced LTD in the cerebellum (Fig. 4 *B*, *D*, and *E*) (66 ± 4% and 69 ± 7% at 25–30 min after CJ-stim in pep-3Y and pep-3A, respectively, $n = 8$ each). Instead, the application of phosphorylated peptides, in which all of the tyrosine residues were phosphorylated (pep-3pY), significantly inhibited LTD induction in WT Purkinje cells (Fig. 4 *C* and *E*) (90 ± 6% at 25–30 min after CJ-stim, $n = 8$, $P = 0.035$ vs. pep-3Y and $P = 0.047$ vs. pep-3A). We did not detect any differences in the EPSC amplitudes just after breaking into whole-cell mode and 9–10 min later in any of the experiments with the peptides (Fig. S5), suggesting that the peptides did not affect basal PF–Purkinje cell synaptic transmission. Because BRAG2 does not bind to phosphorylated GluA2 peptides (14), these results suggested that the BRAG2-Arf6 signaling pathway may not play a major role in CJ-stim–induced LTD in Purkinje cells. Instead, pep-3pY most probably served as a pseudosubstrate for tyrosine phosphatases. Thus, the increased Y876 phosphorylation in *GluD2*-null Purkinje cells inhibited LTD induction mainly by preventing S880 phosphorylation.

***PTPMEG*-Null and *GluD2*-Null Cerebellum Exhibited Similar GluA2 Phosphorylation Patterns.** *GluD2*-null mice show increased phosphorylation of Y876 in GluA2. The C-terminal domain of GluD2

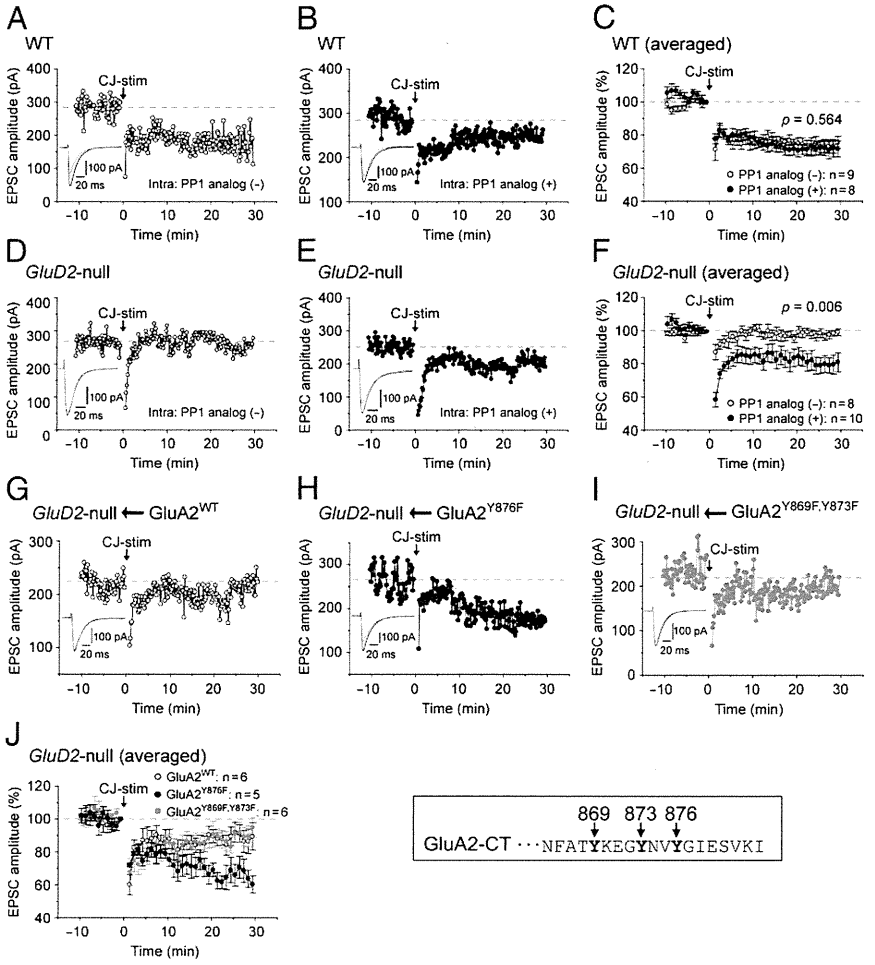

Fig. 3. Dephosphorylation of tyrosine of GluA2 is sufficient to restore LTD induction in *GluD2*-null Purkinje cells. (*A–F*) Inclusion of a PP1 analog in a patch pipette restored LTD in *GluD2*-null Purkinje cells, but it did not affect LTD in WT Purkinje cells. Application of CJ-stim (consisting of 30 cycles of PF stimulation plus Purkinje cell depolarization at 1 Hz) induced LTD in WT Purkinje cells with (+) or without (–) a PP1 analog (10 μM) in patch pipettes (*A* and *B*). CJ-stim successfully induced LTD in *GluD2*-null Purkinje cells with (*E*; +) but not without (*D*; –) a PP1 analog. Collective results (mean and SEM) are shown in *C* and *F*. *Insets* sweeps in *A*, *B*, *D*, and *E* show PF-EPSCs just before (black traces) and 30 min after (gray traces) CJ-stim. (*G–J*) Overexpression of unphosphorable GluA2 subunits restored LTD induction in *GluD2*-null Purkinje cells. Y869, Y873, and Y876 phosphorylation sites (shown on the right in *J*) were replaced with phenylalanine to produce unphosphorable GluA2 mutants termed as $GluA2^{Y876F}$ and $GluA2^{Y869F,Y873F}$. $GluA2^{WT}$, $GluA2^{Y876F}$, and $GluA2^{Y869F,Y873F}$ were overexpressed in *GluD2*-null Purkinje cells by a Sindbis virus vector. CJ-stim–induced LTD was restored in *GluD2*-null Purkinje cells expressing $GluA2^{Y876F}$ (*H*) but not Purkinje cells expressing $GluA2^{WT}$ (*G*) or $GluA2^{Y869F,Y873F}$ (*I*). Collective data (mean and SEM) are shown in *J*. *Insets* sweeps in *G–I* show PF-EPSCs just before (black traces) and 30 min after (gray traces) CJ-stim.

plays a crucial role in LTD induction (3, 4); therefore, we first examined whether the C terminus of GluD2 regulated tyrosine phosphorylation at PF–Purkinje cell synapses by measuring $_{slow}$EPSCs. We used transgenic mice that expressed WT GluD2 (*Tg*WT) or mutant GluD2, which lacked the seven C-terminal residues (*Tg*ΔCT7) on a *GluD2*-null background. In contrast to *GluD2*-null mice, the numbers of PF–Purkinje cell synapses and climbing fiber innervation patterns have previously been shown to be comparable between *GluD2*-null/*Tg*ΔCT7 and *GluD2*-null/*Tg*WT cerebellum (4). Nevertheless, the amplitudes and transferred charges of $_{slow}$EPSCs were significantly smaller in *GluD2*-null/*Tg*ΔCT7 Purkinje cells than *GluD2*-null/*Tg*WT Purkinje cells (Fig. 5*A*) ($P = 0.001$ for amplitudes and $P = 0.001$ for transferred charges). These results indicated that the C terminus of GluD2, to which various intracellular PDZ proteins bind, played a crucial role in the regulation of tyrosine phosphorylation levels in Purkinje cells.

Among the various PDZ proteins that bind to the C terminus of GluD2, we focused on PTPMEG, because it has a catalytically active protein tyrosine phosphatase domain (15) that could potentially serve as a link between the C terminus of GluD2 and the tyrosine phosphorylation levels of Purkinje cells. In addition, *PTPMEG*-null mice displayed impaired motor learning and abrogated LTD (25), although the underlying mechanisms remain unknown. Thus, we first examined the basal phosphorylation levels of GluA2 in *PTPMEG*-null mice. Immunoblot analyses of the synaptosomal fraction revealed that Y876 phosphorylation was significantly increased in *PTPMEG*-null cerebellum compared with WT cerebellum (Fig. 5*B*) (1.84 ± 0.35-fold vs. WT, $n = 10$ each, $P = 0.04$), whereas no differences were observed in the phosphorylation levels of S880 between WT and *PTPMEG*-null cerebellum (Fig. 5*C*) (1.05 ± 0.42-fold vs. WT, $n = 7$ each, $P = 0.85$). Furthermore, K-glu treatment failed to induce a decrease in Y876 phosphorylation (0.99 ± 0.15-fold vs. WT, $n = 15$, $P = 0.97$) and an increase in S880 phosphorylation (0.86 ± 0.14-fold vs. WT, $n = 15$, $P = 0.36$) in *PTPMEG*-null cerebellar slices (Fig. 5*D*). These results were very similar to results that were observed in *GluD2*-null cerebellar slices (Figs. 1*B* and 2*B*), and they suggested that it was PTPMEG that bound to the C ter-

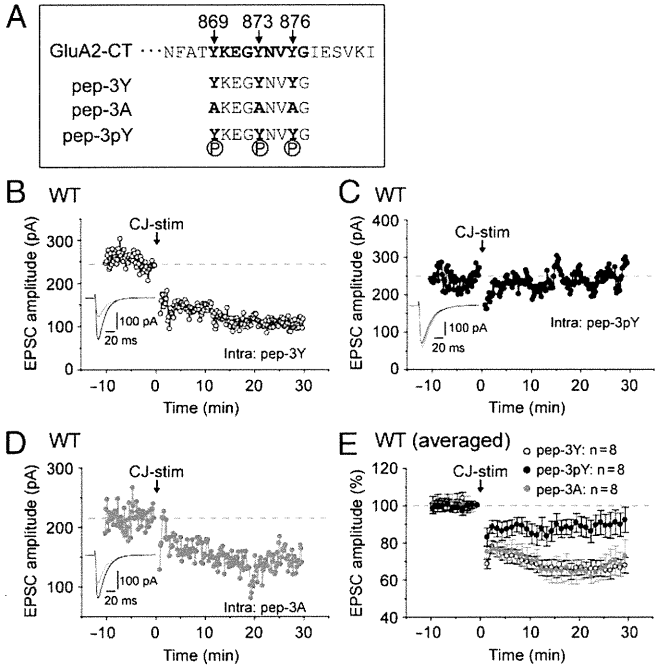

Fig. 4. Dephosphorylation of tyrosine of GluA2 is necessary for LTD induction in WT Purkinje cells. (*A*) Diagram indicating three peptides used in this study. Synthetic peptides correspond to the GluA2 C terminus between positions 869 and 877. Alanine replaced three tyrosine residues in the original peptide (pep-3Y) to produce unphosphorable peptide (pep-3A). All tyrosine residues were phosphorylated in pep-3pY. (*B–E*) LTD is specifically inhibited by pep-3pY, which could serve as a pseudosubstrate for tyrosine phosphatase, included in Purkinje cells. Inclusion of pep-3Y (*B*) or pep-3A (*D*) in patch pipettes did not affect CJ-stim–induced LTD in WT Purkinje cells, but pep-3pY (*C*) inhibited LTD induction. Collective data (mean and SEM) are shown in *E*. *Inset* sweeps show PF-EPSCs before and 30 min after CJ-stim.

minus of GluD2 and regulated the tyrosine phosphorylation at PF–Purkinje cell synapses.

Interactions with PTPMEG Were Necessary and Sufficient for GluD2 to Induce LTD. To further clarify the significance of the interactions between GluD2 and PTPMEG in regulating LTD, we expressed mutant GluD2 that lacked the seven C-terminal residues (GluD2ΔCT7), which did not bind PTPMEG (15) in *GluD2*-null Purkinje cells. As previously reported, unlike WT GluD2 (3), GluD2ΔCT7 did not rescue the impaired LTD in *GluD2*-null Purkinje cells (Fig. 6 *A* and *C*) (90 ± 8% at 25–30 min after CJ-stim, $n = 8$). In contrast, when GluD2ΔCT7-PTP, in which the catalytic phosphatase domain of PTPMEG was fused to the C terminus of GluD2ΔCT7, was expressed in *GluD2*-null Purkinje cells, CJ-stim successfully induced LTD (Fig. 6 *B* and *C*) (76 ± 6% at 25–30 min after CJ-stim, $n = 11$, $P = 0.04$ vs. GluD2ΔCT7). These results suggested that the presence of the phosphatase domain of PTPMEG near GluD2 was sufficient to restore the impaired LTD in *GluD2*-null Purkinje cells.

To examine whether interactions between endogenous GluD2 and PTPMEG were necessary for LTD induction in WT Purkinje cells, we expressed an inactive phosphatase mutant of PTPMEG ($PTPMEG^{DA}$; see next section) with a Sindbis virus vector in WT Purkinje cells. Because CJ-stim no longer induced LTD in WT cells expressing $PTPMEG^{DA}$ (Fig. 6 *D* and *F*) (89 ± 4% at 25–30 min after CJ-stim, $n = 8$), $PTPMEG^{DA}$ probably exerted a dominant-negative effect on endogenous PTPMEG. In contrast, the expression of another mutant ($PTPMEG^{DA}$-ΔPDZ), which lacked the PDZ domain that was necessary for binding to GluD2 (15), no longer inhibited LTD induction in WT Purkinje cells (Fig. 6 *E* and *F*) (66 ± 4% at 25–30 min after CJ-stim, $n = 9$, $P = 0.004$ vs. $PTPMEG^{DA}$). These results indicated that direct interactions between GluD2 and PTPMEG and its phosphatase activity at postsynaptic sites were necessary and sufficient for LTD induction in Purkinje cells.

GluA2, a Substrate for PTPMEG. Finally, to examine whether GluA2 served as a substrate for PTPMEG, we performed a substrate-trapping assay. Various substrates of tyrosine phosphatases have been identified with substrate-trapping mutants, in which mutations in the catalytic center abrogate their enzymatic activity by trapping substrates (26). For example, a substrate-trapping mutant of protein tyrosine phosphatase H1 (PTPH1), which is the most closely related phosphatase to PTPMEG in the phylogenetic tree, has been produced by replacing aspartate with alanine in the catalytic center, and it has been used to identify valosin-containing protein (VCP) as a substrate (27). Thus, we introduced similar mutations in the catalytic center of PTPMEG to produce the possible trapping mutant $PTPMEG^{DA}$, in which alanine (A) replaced aspartate (D). Because many proteins are phosphory-

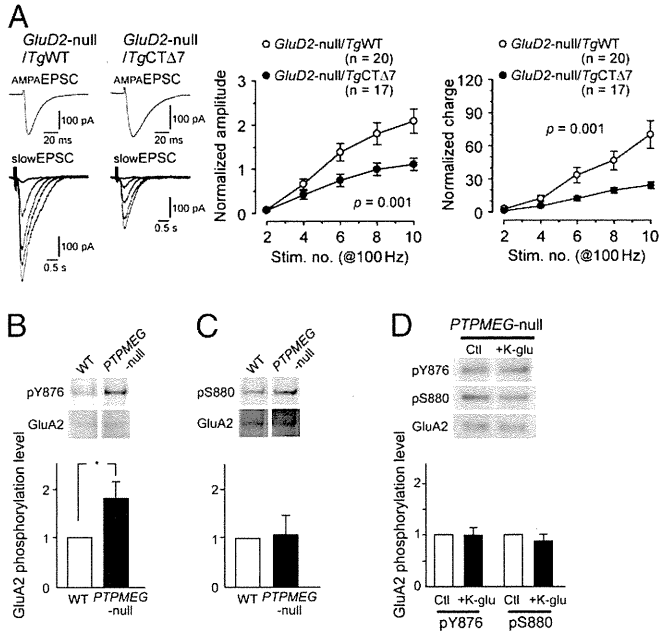

Fig. 5. PTPMEG regulates tyrosine dephosphorylation levels at PF–Purkinje cell synapses. (*A*) Seven C-terminal amino acids of GluD2 determine $_{slow}$EPSC amplitudes in Purkinje cells. $_{slow}$EPSCs were evoked in *GluD2*-null Purkinje cells expressing WT GluD2 transgenes (*GluD2*-null/*Tg*WT) or mutant GluD2 transgenes lacking the seven C-terminal amino acids (*GluD2*-null/*Tg*CTΔ7) as described in Fig. 1*C*. Representative traces are shown in *Left*. Amplitudes and charges of $_{slow}$EPSCs were normalized by amplitudes and charges of $_{AMPA}$EPSCs and plotted against the number of stimulations in *Right*. The bar represents mean and SEM. (*B* and *C*) Basal phosphorylation of Y876 and S880 of GluA2 subunits in *PTPMEG*-null mice. Representative immunoblot images of the synaptosomal fraction of WT and *PTPMEG*-null cerebellum using an antibody against pY876 or pS880 are shown in *Upper*. *Lower* shows intensities of pY876 bands (*B*) or pS880 bands (*C*) in *PTPMEG*-null cerebellum normalized by those band intensities in WT cerebellum. Basal phosphorylation of Y876, but not S880, was significantly increased in *PTPMEG*-null cerebellum. The bar represents mean and SEM. $^*P < 0.05$ ($n = 10$ for Y876; $n = 7$ for S880). (*D*) Chemical LTD stimulus induces no changes at Y876 and S880 sites in *PTPMEG*-null cerebellum. *PTPMEG*-null cerebellar slices were treated with 50 mM KCl plus 10 μM L-glutamate for 5 min (K-glu), and the cell lysates were subjected to immunoblot analyses using phosphorylation-specific antibodies against pY876 and pS880. Representative immunoblot images are shown in *Upper*. In *Lower*, intensities of pY876 and pS880 bands in K-glu–treated slices were normalized to those band intensities in untreated slices. The bar represents mean and SEM ($n = 15$ each).

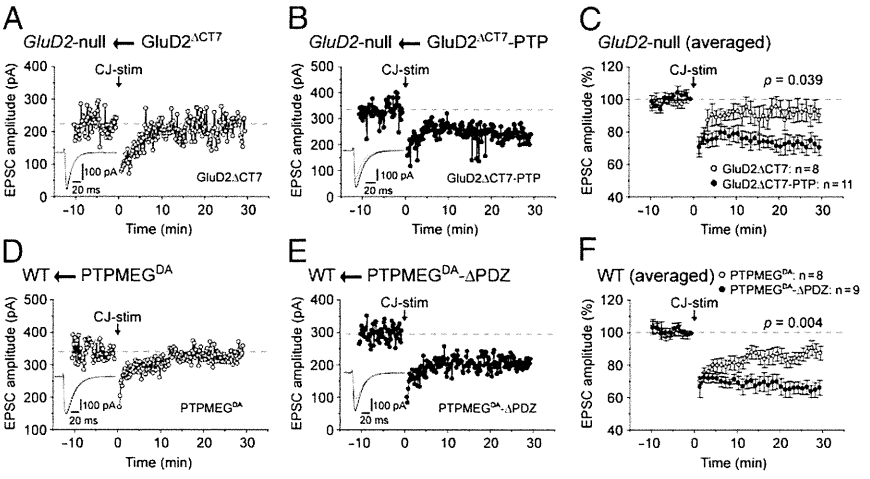

Fig. 6. Interaction of GluD2 with enzymatically active PTPMEG is necessary for LTD induction. (*A–C*) The catalytic domain of PTPMEG was sufficient to restore LTD in *GluD2*-null mice. The catalytic phosphatase domain of PTPMEG was directly fused to the C terminus of a mutant GluD2 lacking the seven C-terminal amino acids (GluD2$^{\Delta CT7}$) to produce GluD2$^{\Delta CT7}$-PTP. GluD2$^{\Delta CT7}$ and GluD2$^{\Delta CT7}$-PTP were expressed in *GluD2*-null Purkinje cells by the Sindbis virus vector. CJ-stim induced LTD in *GluD2*-null Purkinje cells expressing GluD2$^{\Delta CT7}$-PTP (*B*) but not Purkinje cells expressing GluD2$^{\Delta CT7}$ (*A*). Collective data (mean and SEM) are shown in *C*. *Insets* sweeps show PF-EPSCs just before (black traces) and 30 min after (gray traces) CJ-stim. (*D–F*) Interaction with endogenous PTPMEG is necessary for LTD in WT Purkinje cells. A phosphatase-inactive mutant PTPMEG (PTPMEG^{DA}) was produced by replacing aspartate in the catalytic domain with alanine. The PDZ domain, by which PTPMEG binds to the C terminus of GluD2, was further deleted to produce PTPMEG^{DA}-ΔPDZ. PTPMEG^{DA} or PTPMEG^{DA}-ΔPDZ was transduced into WT Purkinje cells using a Sindbis virus vector. CJ-stim–evoked LTD was inhibited in Purkinje cells expressing PTPMEG^{DA} (*D*) but not Purkinje cells expressing PTPMEG^{DA}-ΔPDZ (*E*), indicating that PTPMEG^{DA} bound to GluD2 and replaced endogenous PTPMEG as a dominant-negative molecule. Collective data (mean and SEM) are shown in *F*. *Insets* sweeps show PF-EPSCs just before (black traces) and 30 min after (gray traces) CJ-stim.

lated at tyrosine residues by endogenous tyrosine kinase activities in HEK293 cells, the lysate of HEK293 cells was pulled down by the GST that was fused with the catalytic domain of WT PTPMEG (GST-PTP^{WT}) or PTPMEG^{DA} (GST-PTP^{DA}). As reported for PTPH1 (27), GST-PTP^{DA} but not GST-PTP^{WT} pulled down endogenous VCP in HEK293 cells (Fig. 7*A*). In contrast, unlike VCP, endogenous *N*-ethylmaleimide–sensitive factor, which is a member of the ATPase family that is associated with a variety of cellular activities, did not interact with GST-PTP^{DA} (Fig. 7*A*), indicating that PTP^{DA} specifically trapped its substrates. GST-PTP^{DA} also pulled down GluA2 from the lysate of HEK293 expressing GluA2 (Fig. 7*A*), suggesting that GluA2 was a substrate for PTPMEG.

To examine whether PTPMEG directly dephosphorylated tyrosine residues at the C terminus of GluA2, we performed an in vitro dephosphorylation assay with pep-3pY as a substrate (Fig. 4*A*). GST-PTP^{DA} and GST-PTP^{CS}, having cysteine (C) residue in the catalytic center that was replaced with serine (S), were used as PTPMEG mutants with reduced phosphatase activities. Isobaric tag-based mass spectrometric quantification of the phosphorylation of pep-3pY peptides revealed that all tyrosine residues were dephosphorylated by incubation with GST-PTP^{WT} (0.06 ± 0.02-fold compared with pep-3pY peptides incubated with GST only, $n = 6$) (Fig. 7*B*). In contrast, the relative phosphorylation levels of pep-3pY, which was incubated with GST-PTP^{DA} (1.1 ± 0.3, $n = 6$) or GST-PTP^{CS} (1.0 ± 0.1, $n = 6$), were significantly higher than those levels treated with PTP^{WT} (WT vs. DA or CS, $P < 0.05$) (Fig. 7*B*). These results indicated that the phosphorylated tyrosine residues in the GluA2 C terminus were directly dephosphorylated by PTPMEG in vitro.

To further confirm that PTPMEG dephosphorylated Y876 in GluA2 in a cellular context, we examined whether full-length PTPMEG dephosphorylated GluA2 in HEK293 cells. Immunoblot analyses of the lysate of HEK293 cells transfected with GluA2 revealed that GluA2 was weakly phosphorylated at Y876 by endogenous tyrosine kinases in HEK293 cells. We found that Y876 phosphorylation levels were significantly higher in HEK293 cells that coexpressed a phosphatase-inactive mutant PTPMEG^{DA} (3.6 ± 0.9-fold vs. PTPMEG^{WT}, $n = 8$ each, $P < 0.05$) (Fig. 7*C*) than cells that coexpressed PTPMEG^{WT} or an empty vector (1.4 ± 0.3-fold vs. PTPMEG^{WT}, $n = 8$ each, $P < 0.05$) (Fig. 7*C*). There was no statistically significant difference in the phosphorylation levels of Y876 between the cells expressing PTPMEG^{WT} and an empty vector, suggesting that endogenous tyrosine phosphatase dephosphorylated Y876 in HEK293 cells. These results indicated that Y876 in GluA2 served as a direct substrate for PTPMEG.

Discussion

LTD at PF–Purkinje cell synapses is believed to play important roles in motor learning in the cerebellum, and it has been shown to absolutely require functional GluD2 in Purkinje cells (28). Nevertheless, how and why GluD2 regulates LTD in the cerebellum remain elusive. In this study, we show that the basal phosphorylation levels of Y876 in GluA2 were increased (Fig. 1) and that the phosphorylation at Y876 prevented subsequent phosphorylation at S880 (Fig. 2), which has been shown to be an essential phosphorylation site for AMPA receptor endocytosis during LTD in both hippocampus (6, 7) and cerebellum (8–10). Dephosphorylation of Y876 restored AMPA receptor endocytosis (Fig. 2) and LTD (Fig. 3) in *GluD2*-null mice. An association of PTPMEG with the C terminus of GluD2 was necessary and sufficient for LTD induction in Purkinje cells (Figs. 3, 4, 5, and 6). Furthermore, PTPMEG directly dephosphorylated Y876 phosphorylation of GluA2 (Fig. 7). Therefore, we propose that GluD2 serves as a master switch in gating the inducibility of LTD by coordinating the interactions between the two phosphorylation sites in GluA2 through its interactions with PTPMEG (Fig. 8).

Interactions Between Y867 and S880 Phosphorylation During LTD. Whether tyrosine phosphorylation is involved in cerebellar LTD has been controversial. In early studies, cerebellar LTD has been reported to be blocked by broad-spectrum tyrosine kinase inhibitors, such as genistein and lavendustin A, suggesting that LTD depends on tyrosine phosphorylation events (29, 30). In contrast, the application of a more specific Src inhibitor PP2 to the bath solution (31) or PP1 to a patch pipette (Fig. 3 *A–C*) did not affect